Lung-mimicking hydrogel culture system reproduces several tuberculosis phenotypes and demonstrates pyrazinamide efficacy

Vishal K. Gupta[1], Abhirami P.S.[1], Jyothsna K.M.[2], Sharumathi Jeyasankar[1], Varun Raghunathan[2], Rachit Agarwal[1*]

[1]*Centre for BioSystems Science and Engineering, Indian Institute of Science, Bengaluru, India.*

[2]*Department of Electrical Communication Engineering, Indian Institute of Science, Bengaluru, India.*

[*] Corresponding author email: rachit@iisc.ac.in (Rachit Agarwal)

Keywords: Collagen hydrogels, cord formation, foamy macrophages, pyrazinamide

Abstract:

Faithful mimics of tuberculosis (TB) infection are needed to provide mechanistic insights into the complex host-pathogen interactions and for accelerating drug discovery. The current *in vitro* models provide a short duration to investigate, present divergent transcriptional signatures to human infections, and are unreliable drug discovery platforms. We developed a 3D collagen culture system mimicking the lung microenvironment (collagen fibres, pore size and stiffness), where we incorporated *Mycobacterium tuberculosis* (Mtb) infected THP-1 or primary monocytes. Dual RNA-sequencing revealed high similarity with human infections. Phenotypes observed in humans, such as foamy macrophages and mycobacterial cords (never seen in any other *in vitro* culture system), were reproduced in our culture system. The system overcomes many challenges associated with the traditional platforms, including showing remarkable efficacy with clinically relevant concentrations of first-line anti-TB drug pyrazinamide, not seen in any other *in vitro* model, making it reliable, readily adoptable for tuberculosis studies and drug screening.

Introduction:

In 2021, the World Health Organization (WHO) reported 10 million new TB cases, which resulted in 1.5 million deaths (*1*). TB is transmitted through aerosols containing the bacteria generated by an infected individual. Upon reaching the alveolus of the new host, the bacteria infect the resident alveolar macrophages, which migrate to the lung interstitium and recruit circulating monocytes and other immune cells, leading to the formation of granuloma (*2*, *3*). Monocytes and macrophages carry a large reservoir of bacteria *in vivo* and play critical roles in the host response to mycobacterial infection (*4*-*6*). These cells are important for studying host-pathogen interaction and hence have been widely employed in the field (*7*-*9*).

Conventionally, *in vitro* Mtb infection experiments are performed in two-dimensional (2D) tissue culture systems on polystyrene plates, using primary human monocyte-derived macrophages, mouse bone marrow-derived macrophages (BMDMs), and human THP-1 macrophages (*10*). These studies have contributed to our understanding of complex processes such as the arrest of phagosomal maturation, activation of innate immune responses, and the underlying mechanisms modulating various cell death pathways(*7*). However, the existing culture systems have critical drawbacks: First, monolayer (2D) cultures fail to provide the natural environments for the cells, wherein cells are usually subjected to very stiff surfaces (~10 GPa), resulting in many dysregulated cellular processes(*11*). Second, host cell viability after Mtb infection is low in 2D cultures, limiting the length of the experiments to 4-6 days. Mtb is a slow-growing pathogen (median doubling time of >100 h)(*12*) that modulates host responses to help its survival over several days/weeks. The conventional 2D platforms fail to recapitulate these intricate host-pathogen dynamics. Third, substantial variation exists in gene expression between infected cells in 2D cultures and human infection (*13*). Fourth, the current systems seem unreliable as platforms to screen TB drugs. For instance, pyrazinamide, a first-line anti TB drug, has shown little to no efficacy in any previously used *in vitro* culture systems

at clinically relevant concentrations but is extremely effective *in vivo* (*14*). Similarly, several clinical trials with potential TB drugs and treatment regimens have failed despite showing promise in the initial stage of testing (*15*). These limitations underscore the need to develop better and more representative culture systems to accurately study host-mycobacteria interactions. An ideal culture system should (a) provide a longer timeframe (~weeks) for studying host-pathogen dynamics in TB; (b) be able to better recapitulate the genotypic and phenotypic characteristics of human infection; (c) be a more reliable platform for advancing drug susceptibility studies; (d) be simple with accessible components to enable easy and widespread adoption in the field.

In recent years, three-dimensional (3D) *in vitro* models have gained interest in the field (*16-18*). 3D models provide a more realistic representation of human tissues than their 2D counterparts, as they mimic cells *in vivo* that are surrounded by other cells and the extracellular matrix (ECM) (*19*). 3D models of Mtb infection have been developed using natural and synthetic polymers and peripheral blood mononuclear cells (PBMCs) to model TB granuloma (*17, 18*). However, these systems have two major drawbacks: first, they either use synthetic components in their constructs. The presence of natural ECM results in a more faithful recapitulation of viability, proliferation, differentiation, and response to a stimulus compared to the 2D systems (*20*). Second, they depend on access to specialized equipment (to form gels) and hospitals (to obtain primary cells). The reliability and ease of adoption of these systems are thus limited.

We have synthesized hydrogels made of Collagen I, the primary extracellular component in the human lungs, having a micromechanical environment similar to human lung tissue. The collagen gels are easy to form and do not require any specialized equipment. These gels support the culture of THP-1 and primary human monocytes, with the cells sustaining Mtb infection beyond 3 weeks. Dual RNA-sequencing of the host and pathogen transcriptomes from collagen

gels showed that the gene expression profiles of the mammalian and bacterial cells infected in our collagen gels mimic human infection significantly better than in 2D cultures. The monocytes in the infected gels differentiated into macrophages and accumulated lipid bodies, a phenotype observed in macrophages in human TB granulomas (*21*). The longevity of this culture system enabled us to see bacterial growth in the form of cords, a phenotype observed *in vivo* (*5, 22-24*) but not in any *in vitro* macrophage infection model. Finally, our culture system emerged as an excellent drug testing platform, shown by the efficacy of pyrazinamide, an anti-TB drug that is ineffective in any other *in vitro* model, at concentrations used clinically (C_{max} of 50 µg/mL). Rapid and widespread adoption of this system is thus likely and would not only aid drug discovery and development but also shed new insights into the complex host-pathogen interactions underlying TB infections.

Results:

1. Characterization of collagen gels revealed their micromechanical similarity with human lungs and cytocompatibility:

As the Mtb infection initiates in the lung, which primarily comprises of ECM network of collagen I, we synthesized and tuned a physically crosslinked collagen I hydrogel that can mimic the biochemical and biophysical cues of human lungs (*25, 26*). To characterize the mechanical microenvironment, collagen gels were analyzed using Atomic Force Microscopy (AFM). The Young's modulus obtained was 0.64 kPa ± 0.12 kPa and 2.1 kPa ± 0.3 kPa for 1 mg/mL and 2 mg/mL collagen gels, respectively (**Fig. 1A**). Since the modulus of healthy human lung tissue is in range of 1.4 to 7 kPa(*27, 28*), we chose 2 mg/mL collagen gels for all subsequent assays. Next to characterize whether these gels can mimic the fibrillar structure of ECM in human lungs, the collagen gels were imaged using second harmonic generation (SHG)

imaging, a label-free imaging technique based on collagen's native property to generate the second harmonics when the wavelength of incident light beam is more than 800 nm (*29*). SHG imaging showed distinct fibrils (**Fig. 1B)** and morphologically mimicked lung ECM microenvironment (*25, 30*)**.** The average pore diameter in gels with final collagen I concentration of 2 mg/mL was 8.45 $\mu m^2 \pm 2.37\ \mu m^2$, allowing cells to move through the matrix. The ECM is critical to cell viability as cellular detachment from ECM alters their processes such as metabolism. The separation from ECM also leads to cell death due to anoikis (*31*). Collagen plays a critical role in the progress of TB infection as its degradation results in reduced cell viability leading to the caseation of TB granuloma (*32*). We first tested the cytocompatibility of collagen gels for THP-1 cells by culturing them for 10 days. Minimal cytotoxicity was observed by Calcein -AM – propidium iodide (PI) staining (**Fig. 1C and 1D)**.

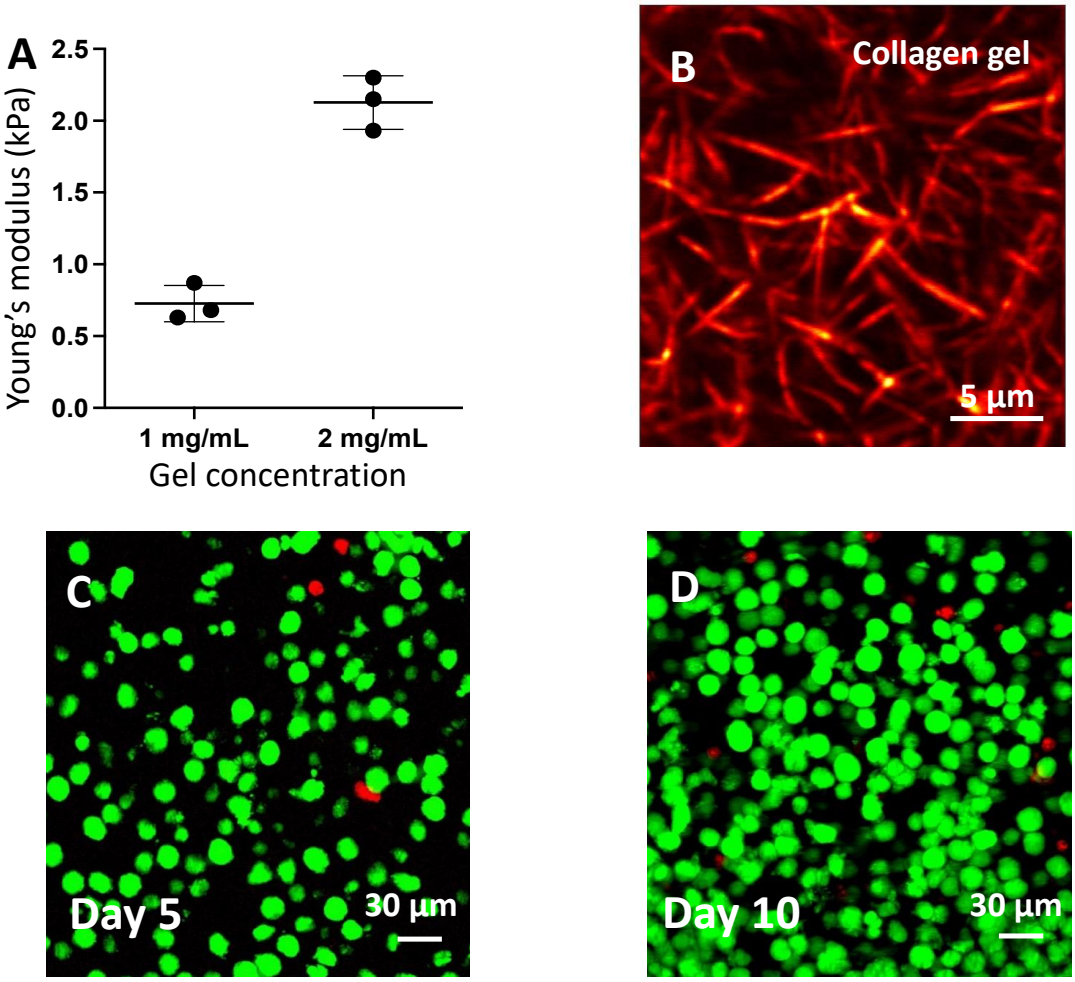

Fig. 1 Collagen gels mimic the micromechanical environment of lungs and are cytocompatible. (**A**) Young's modulus of 1 mg/mL and 2 mg/mL collagen gels. Data in graphs represent the mean ± s.d. (n = 3). (**B**) Representative SHG image of 2 mg/mL collagen gel. Scale: 5 µm. (**C**) and (**D**) Representative images of Calcein-AM (green, live) – PI (red, dead) stained cells images in collagen gels on days 5 and 10, respectively. Scale: 30 µm.

2. Collagen gels support monocyte infection and cell survival for a prolonged duration:

We characterized the infection percentages at a range of MOIs (0.1- 40) in PMA-treated THP-1 macrophages (2D infection) and for our 3D model. To achieve infection in 3D, THP-1 monocytes and Mtb were added to the collagen gel before polymerization. Successful infection was achieved upon incubating THP-1 cells with Mtb in the hydrogels for 12 h, after which the gels were treated with a mammalian cell impermeable antibiotic (amikacin sulfate) to eliminate extracellular bacteria (*33*). An MOI of 40 in the 3D model resulted in a similar intracellular infection percentage as an MOI of 1 in 2D infection (**Supplementary Fig. S1**) and was used for further experiments. Harmonizing the initial infection percentages in 2D and 3D was done for easy subsequent comparisons. We also found that infecting undifferentiated monocytes with Mtb (MOI of 40) in the absence of collagen gels resulted in very few THP-1 cells getting infected (**Supplementary Fig. S2)**, which highlights the importance of collagen in mediating host-Mtb infection.

A major limitation of the existing 2D infection models is the relatively smaller time frame available for carrying out experiments (*34*). An infection with MOI of 1 resulted in viable host cells for approximately 7 days, beyond which the cell viability dropped below 10% (**Supplementary Fig. S3)**. This is a major constraint for long-term mechanistic and drug studies as Mtb is a slow-growing pathogen with a median doubling time >100 h inside

mammalian cells (*12*). Post-infection, the bacteria take 1-2 days to adapt to the mammalian system, (*35*) which further reduces the available time for assays by nearly 25-30%.

In the infected collagen 3D environment, we could successfully culture cells for 22 days (**Fig. 2B**). At various time points, the viability and infection rates were analyzed using flow cytometry. 8 days post-infection, 60±3% cells were viable, and the corresponding numbers for 15- and 22 days post-infection were 63±7% and 40±9%, respectively. After 8, 15, and 22 days, the infection rates were 8±0.9%, 10±1.3%, and 30±12.4%, respectively. We also performed a colony forming unit (CFU) assay using H37Rv transformed with the pBP10 clock plasmid (*36*) (replication clock plasmid) to understand the bacterial growth kinetics (**Fig. 2C & 2D)**. We found that during the first 2 days of infection, the CFUs reduce with minimal bacterial replication as seen from rate of loss of the replication clock plasmid, which could be due to the adaptation of bacteria to the system. As time progresses, Mtb grows (with a corresponding loss in clock plasmid) in the THP-1 cells cultured in collagen gels, and hence the proportion of infected cells increases with time while the overall viability of mammalian cells decreases. Thus, this platform offers a significantly longer window for testing drugs and studying host-pathogen interaction during infection than any other *in vitro* culture systems.

During lung infection, monocytes get recruited to the site of inflammation and differentiate into macrophages (*37, 38*). In the collagen culture system, to determine whether monocytes were differentiating into macrophages upon Mtb exposure, cells were stained with CD68, a specific intracellular marker for macrophages (*39*). Mtb infection resulted in CD68 expression in nearly 52% of cells 10 days post-infection (**Fig. 2E-F**) compared to only 14% in uninfected gels. We then analyzed the Mtb positive vs bystander cells in the infected conditions using flow cytometry to determine if all cells were uniformly differentiated into macrophages. Nearly all Mtb-infected cells were positive for CD68 (~95%) (**Supplementary Fig. S4**), implying that infection resulted in the differentiation of monocytes to macrophages in collagen gels. We also

observed that about 42% of the bystander (uninfected) population showed CD68 expression (**Supplementary Fig. S4**), implying that the infected microenvironment also promoted differentiation of THP-1 monocytes to macrophages.

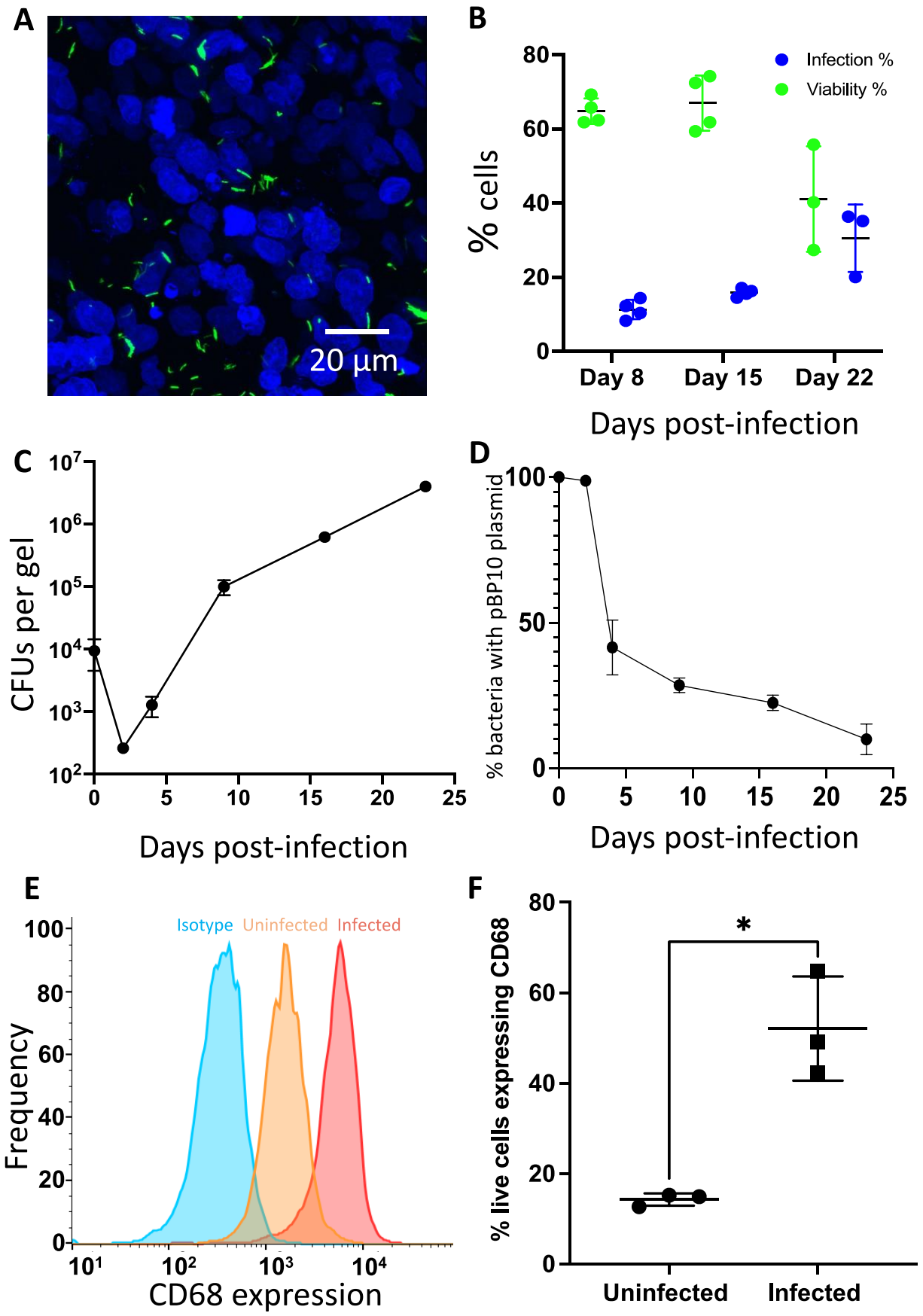
A
20 µm
B
Infection %
Viability %
% cells
80
60
40
20
0
Day 8
Day 15
Day 22
Days post-infection
C
CFUs per gel
10^7
10^6
10^5
10^4
10^3
10^2
0
5
10
15
20
25
Days post-infection
D
% bacteria with pBP10 plasmid
100
50
0
0
5
10
15
20
25
Days post-infection
E
Isotype
Uninfected
Infected
Frequency
100
80
60
40
20
0
10^1
10^2
10^3
10^4
CD68 expression
F
% live cells expressing CD68
80
60
40
20
0
*
Uninfected
Infected

Fig. 2 Collagen gels support THP-1 cell infection with Mtb over a long duration. (A) Fluorescence microscopy images of infected THP-1 cells in collagen gel, GFP-Mtb (H37Rv). (**B**) The percentage of live THP-1 cells (green), and THP-1 cells infected with H37Rv-GFP (blue) at various intervals (n = 4). (**C**) Kinetics of bacterial growth (CFUs) in the 3D collagen culture system (n = 3). (**D**) The percentage of intracellular bacteria containing the replication clock plasmid (pBP10) at various time points in the infected collagen gels, represented by CFUs (mean ± s.d.) on kanamycin vs non-kanamycin plates (n = 3). (**E**) Representative histogram showing CD68 expression: cells from infected gels (red), isotype control (blue), cells from uninfected gels (orange) (n = 3). (**F**) Plot showing percentage of live CD68 positive cells in uninfected and infected gels (n = 3). For **F**, data in graph represents the mean ± s.d., and p value was determined by a two-tailed unpaired t-test with Welch's correction using GraphPad Prism software. p-value < 0.05 was considered significant. *p=0.0282

3. Dual RNA sequencing revealed similarities in gene expression between mammalian cells of the collagen hydrogel system and human TB granulomas

We carried out dual RNA sequencing to dissect the host-pathogen interaction mechanisms by identifying their transcriptomic differences in the collagen gels 14 days post-infection and the differentially expressed mammalian and Mtb genes are listed in **Supplementary Table 1**. The differentially expressed gene (DEG) distribution for mammalian genes is shown in **Fig. 3A**. Gene expression patterns from our system were compared with the expression profiles of an infected human 2D macrophage cell line (GSE162729)/ primary cells (GSE174566) and with human infection (caseous lung granuloma (GSE20050) and lymph-node granuloma (GSE17443). The 3D collagen culture system had the highest number of commonly regulated genes with human caseous TB granuloma (*21*) (gene list: **Supplementary Table 2**) and with human lymph node granuloma (*13*) (gene list: **Supplementary Table 3**) as compared with the

other 2D infection models (**Fig. 3B**), which had less than 1 % commonly regulated genes. The top upregulated and downregulated DEGs common between the lymph node granuloma and the 3D collagen culture system showed similar regulation patterns (**Fig. 3C**). To better understand the functional relevance of such a gene expression pattern, we also performed a REACTOME pathway gene set enrichment analysis for the differentially regulated genes in various models and found a significant overlap in both the upregulated and downregulated pathways between the human TB granulomas and 3D collagen culture system (**Supplementary Fig. S5**). The upregulated REACTOME pathways in the collagen model corresponded to ECM organization, signal transduction, while the downregulated ones were associated with protein metabolism, organelle biogenesis, and maintenance, among others. The 2D models, on the other hand, showed contradictory regulation of many pathways such as ECM organization, integrin cell-surface interactions, interleukin and interferon signaling, or those associated with the cell cycle, compared to the human TB granulomas. These results collectively indicated how our system significantly recapitulated the Mtb-mediated *in vivo* pathway regulations.

The transcriptomic analysis of Mtb from the infected collagen gels identified 460 significantly differentially regulated genes (|log2fc|>1, FDR<0.05, 241 upregulated and 219 downregulated, **Supplementary Table 4**) when compared to the planktonic bacteria cultured in 7H9 medium. Functional categorization revealed the upregulated genes involved in crucial infection-related functions such as virulence and adaptation and cell wall processes, among others (**Fig. 4A**). Given the lack of robust Mtb transcriptomic data from human infections, the comparisons were made with observations from infected mice (*9*), which showed 114 genes to be similarly regulated in our hydrogels (55 genes upregulated and 59 genes downregulated) (**Supplementary Table 5**). However, Mtb transcriptome from THP-1 macrophages infected for 24 h in 2D (*40*) showed only 21 genes (all upregulated) to be similarly regulated compared to mice infection (**Supplementary Table 5**). This Mtb transcriptomic signature in 2D (from

early time points as compared to 3D) pointed towards the pathogen's adaptation to the mammalian cells, wherein, genes associated with zinc ion homeostasis, type VII secretion system, and membrane repair were significantly upregulated. Our analyses also revealed a large variation between the Mtb transcriptomes from 2D infected cells (*40*) and the collagen hydrogels, which could probably be attributed to the time spent by the pathogen in the host (24 h in 2D vs 14 days in collagen gels, **Supplementary Table 5**).

We then looked at the functional analyses of the Mtb transcriptome in the model and found significant upregulation of most of the genes of the Kstr2 regulon (**Fig. 4B**), indicating high cholesterol-associated metabolism of the pathogen (*9*). Intriguingly, we found the upregulation of the mce1 operon genes (*mec1A, mce1B, mce1C, mce1F, mce1R*) (**Fig. 4B**), which are similarly regulated *in vivo*, but oppositely regulated in traditional 2D infection cultures; genes of this operon are hypothesized to be involved in modulating host response to facilitate persistence (*41*) and fatty acid transport (*42, 43*). Moreover, we also found upregulation of genes involved in lipid degradation (*lipL, plcC*), TCA cycle, and fatty acid β-oxidation (*icd1, Rv0893c, echA20*), highlighting the dependence of Mtb on cholesterol and fatty acid utilization in our model, a characteristic of the pathogen's metabolism in the interstitial and alveolar macrophages, respectively, *in vivo* (*9, 44*). Furthermore, we also found upregulation of genes of the tryptophan synthase operon (*trpA, trpB, trpC*). Mtb has the ability to synthesize tryptophan, thus counteracting the attempts by T-cells to starve the pathogen of this essential amino acid (*45*). These results collectively indicate a robust gene signature similarity of Mtb from our system with that from established *in vivo* infection models, such as in mice, while highlighting the drawbacks of using the conventional 2D systems for functional studies. Furthermore, these observations point to the gaps in our understanding of the pathogen's behavior in humans, warranting more in-depth transcriptomic studies. Overall, the 3D collagen

culture system was able to capture multiple mechanisms underlying Mtb infection-associated host-pathogen dynamics significantly better than the current *in vitro* platforms.

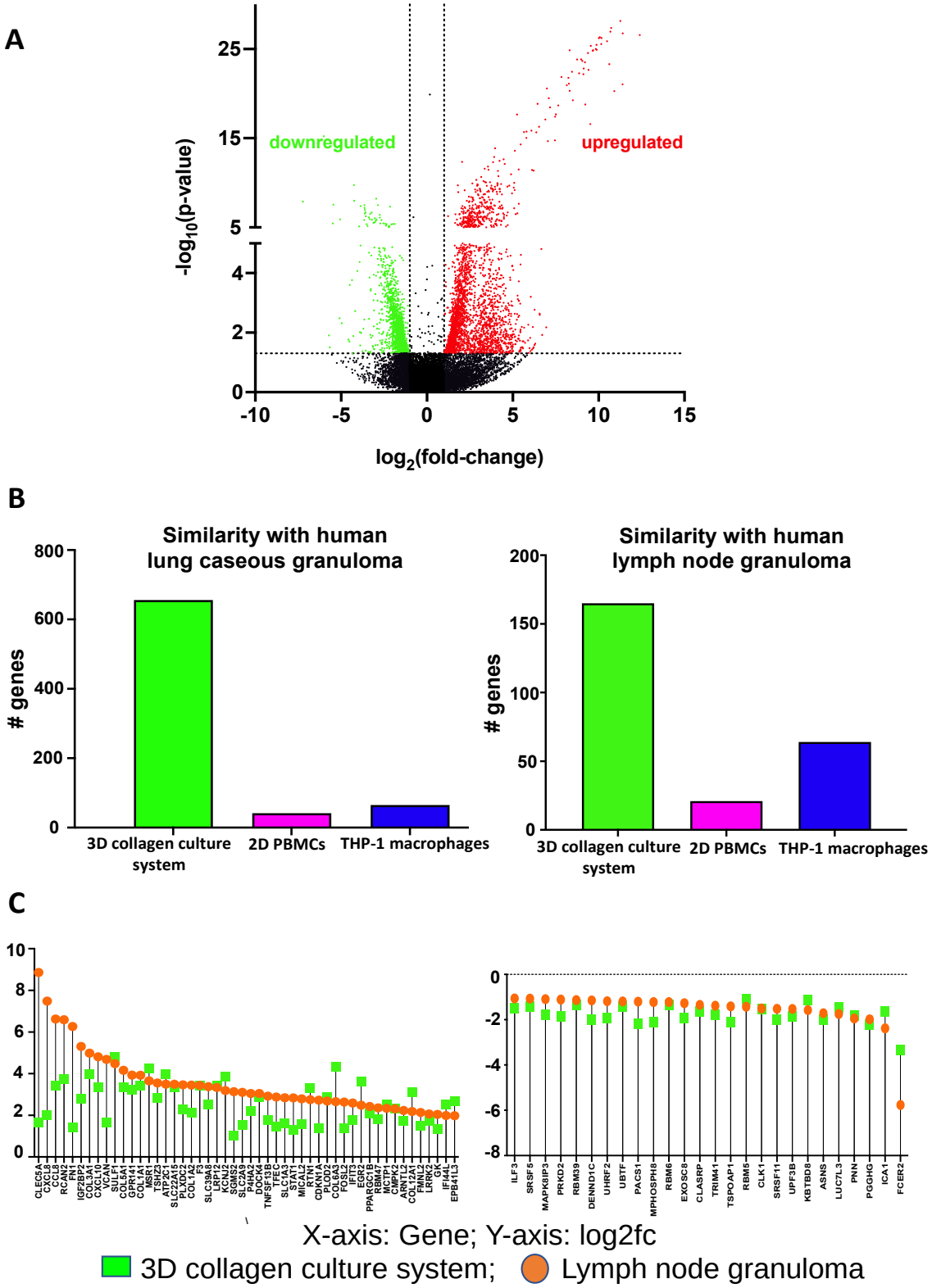

Fig. 3 RNA-sequencing of the mammalian cells from the infected collagen gels show maximum similarity with *in vivo* systems. (**A**) A volcano plot of differentially expressed THP-1 genes between uninfected hydrogels and the Mtb infected hydrogels (red: significantly upregulated, green: significantly downregulated, black: non-regulated) (**B**) Quantification of common genes between the various models and the primary TB granulomas (green: 3D collagen culture system, pink: 2D PBMCs, blue: 2D THP-1 macrophages). (**C**) Extent of regulation of the top upregulated genes and downregulated genes common to lymph node granuloma and the 3D collagen culture system.

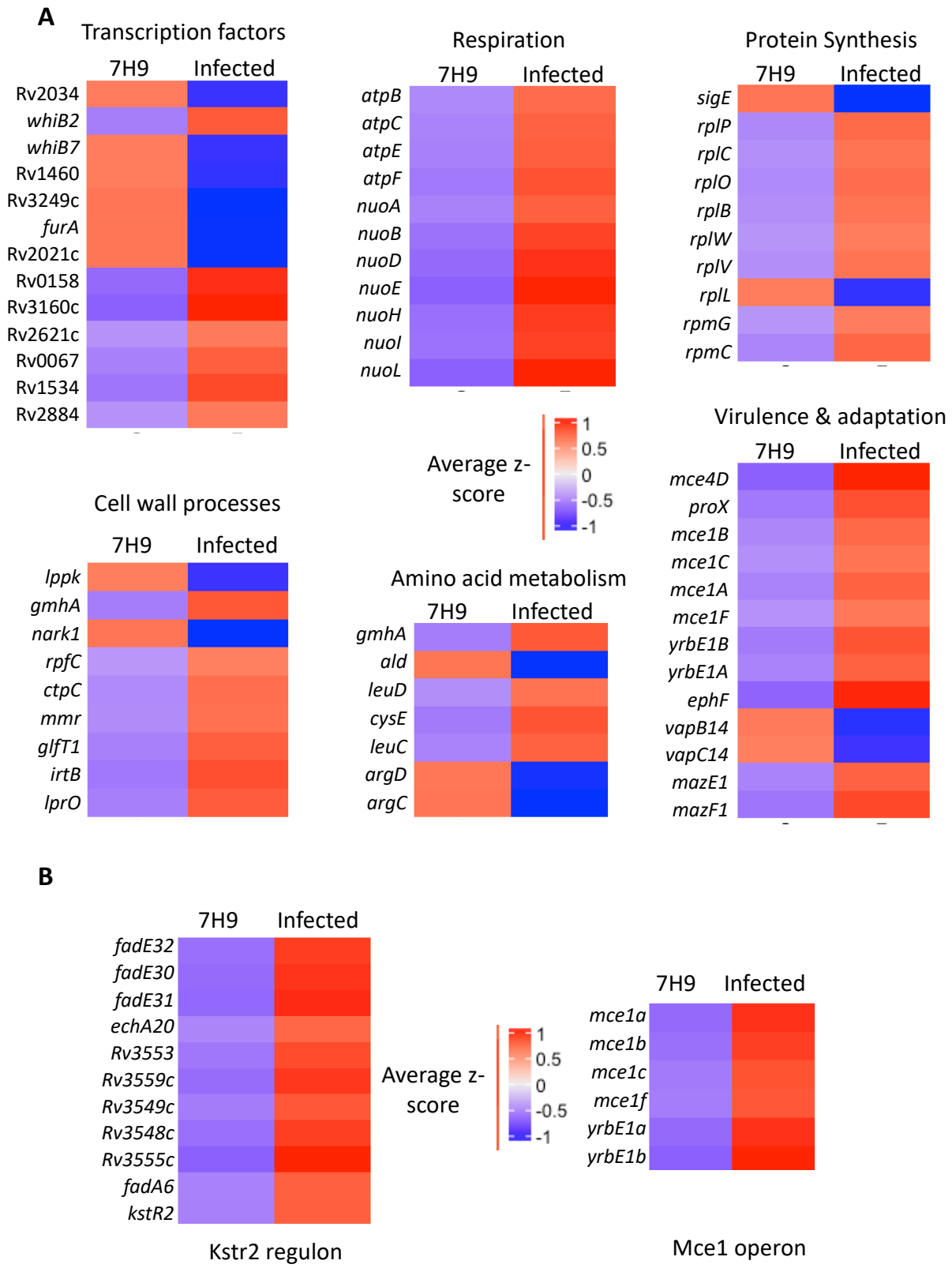
A
Transcription factors
7H9
Infected
Rv2034
whiB2
whiB7
Rv1460
Rv3249c
furA
Rv2021c
Rv0158
Rv3160c
Rv2621c
Rv0067
Rv1534
Rv2884
Respiration
7H9
Infected
atpB
atpC
atpE
atpF
nuoA
nuoB
nuoD
nuoE
nuoH
nuoI
nuoL
Protein Synthesis
7H9
Infected
sigE
rplP
rplC
rplO
rplB
rplW
rplV
rplL
rpmG
rpmC
Average z-score
1
0.5
0
-0.5
-1
Virulence & adaptation
7H9
Infected
mce4D
proX
mce1B
mce1C
mce1A
mce1F
yrbE1B
yrbE1A
ephF
vapB14
vapC14
mazE1
mazF1
Cell wall processes
7H9
Infected
lppk
gmhA
nark1
rpfC
ctpC
mmr
glfT1
irtB
lprO
Amino acid metabolism
7H9
Infected
gmhA
ald
leuD
cysE
leuC
argD
argC
B
7H9
Infected
fadE32
fadE30
fadE31
echA20
Rv3553
Rv3559c
Rv3549c
Rv3548c
Rv3555c
fadA6
kstR2
Kstr2 regulon
Average z-score
1
0.5
0
-0.5
-1
7H9
Infected
mce1a
mce1b
mce1c
mce1f
yrbE1a
yrbE1b
Mce1 operon

Fig. 4 RNA sequencing analysis of bacteria from collagen culture systems show important differences compared to planktonic bacteria. (**A**) Heat maps for the normalized z-scores of the differentially regulated Mtb genes belonging to various functional categories comparing planktonic bacteria grown in 7H9 medium with bacterial cells cultured in 3D collagen gels with mammalian cells (source: Mycobrowser, École Polytechnique fédérale de Lausanne). Genes were considered differentially expressed on the basis of |log2fc| ≥1 and FDR of ≤ 0.05. (**B**) Heat maps for the normalized z-scores of the genes involved in Kstr2 regulon and the mce1 operon

4. THP-1 cells accumulate lipid bodies in response to infection and Mtb forms cord-like structures in the infected gels:

Next, we focused on deciphering the Mtb-mediated metabolic alterations. Mtb can persist in the host for long durations and possesses the ability to switch the source of energy required for its metabolism (*46*) (*47*). In the initial stages of infection, the pathogen relies on glucose and fatty acids for its metabolism; however, as the infection progresses, fatty acids and cholesterol become the major energy source (*46*). Thus, Mtb induces metabolic reprogramming in the macrophages to accumulate triglycerides, leading to the formation of foamy macrophages, a hallmark of human primary granuloma (*47*). In 2D system, owing to the shorter duration of infection, the increase in accumulation of lipids by the infected mammalian cells is not significant **(Supplementary Fig. S6)**. To see if similar to *in vivo* infection conditions, foamy macrophages were generated in our 3D culture system, the uninfected and infected collagen gels were stained for neutral lipids with BODIPY (*48*). The cells in the infected gels showed a higher abundance of lipid droplets compared to uninfected (**Fig. 5A-B**). Infected gels had 3-4 folds higher signal on days 7 and 10 post-infection compared to uninfected gels (**Fig. 5C**). Additional confirmation by flow cytometry showed that 10 days post-infection, the cells from

the infected gels had nearly 3-4 times higher BODIPY signal compared to those from the uninfected ones (**Fig. 5D**). Transcriptomic data from human caseous granuloma (GSE20050) showed upregulation of 55 genes involved in lipid metabolism (*21*) and nearly a third of these genes were also upregulated in our culture system; this is in contrast to the negligible overlap with the current *in vitro* 2D models, further validating the efficiency with which our system mimics *in vivo* infections **(Fig. 5E).**

Mtb can aggregate and form cord-like structures, known as cording, which is regularly observed *in vivo* (*22, 23, 49, 50*) and is associated with the bacteria's virulence and immune escape mechanism. It has been established that cording correlates to the growth of Mtb in the extracellular milieu *in vivo* (*50, 51*). Similarly, we also observe bacterial cording at later time points in the culture system (post 2 weeks) **(Fig. 5F)**, thereby enabling the bacteria to prevent phagocytosis once they become extracellular upon killing the host cell (*52, 53*). Previous *in vitro* studies have shown that human lymphatic endothelial cells (*53*) are conducive for cord formation by Mtb, 3-4 days post-infection. However this phenotype has never been shown in an *in vitro* macrophage infection culture system. Host cell autophagy is an important defense mechanism against intracellular pathogens, and the upregulation of autophagic genes and pathways in our dual RNA sequencing data points towards such a phenomenon also occurring in our system, which the bacteria successfully evade by cording (*53*). Furthermore, in our Mtb transcriptomic data, upregulation of the gene *fbpC*, a member of the antigen 85 family of proteins that confer fibronectin binding affinity and maintain the cell wall integrity of Mtb by synthesizing alpha trehalose-dimycolate (TDM, cord factor) (*54*), elucidated the molecular basis of cording in our system. Thus our 3D culture system could capture a crucial Mtb phenotype that aids infection, not observed earlier in other *in vitro* systems, and often used as a marker for the limitation of macrophages to control bacterial growth *in vivo* (*22*).

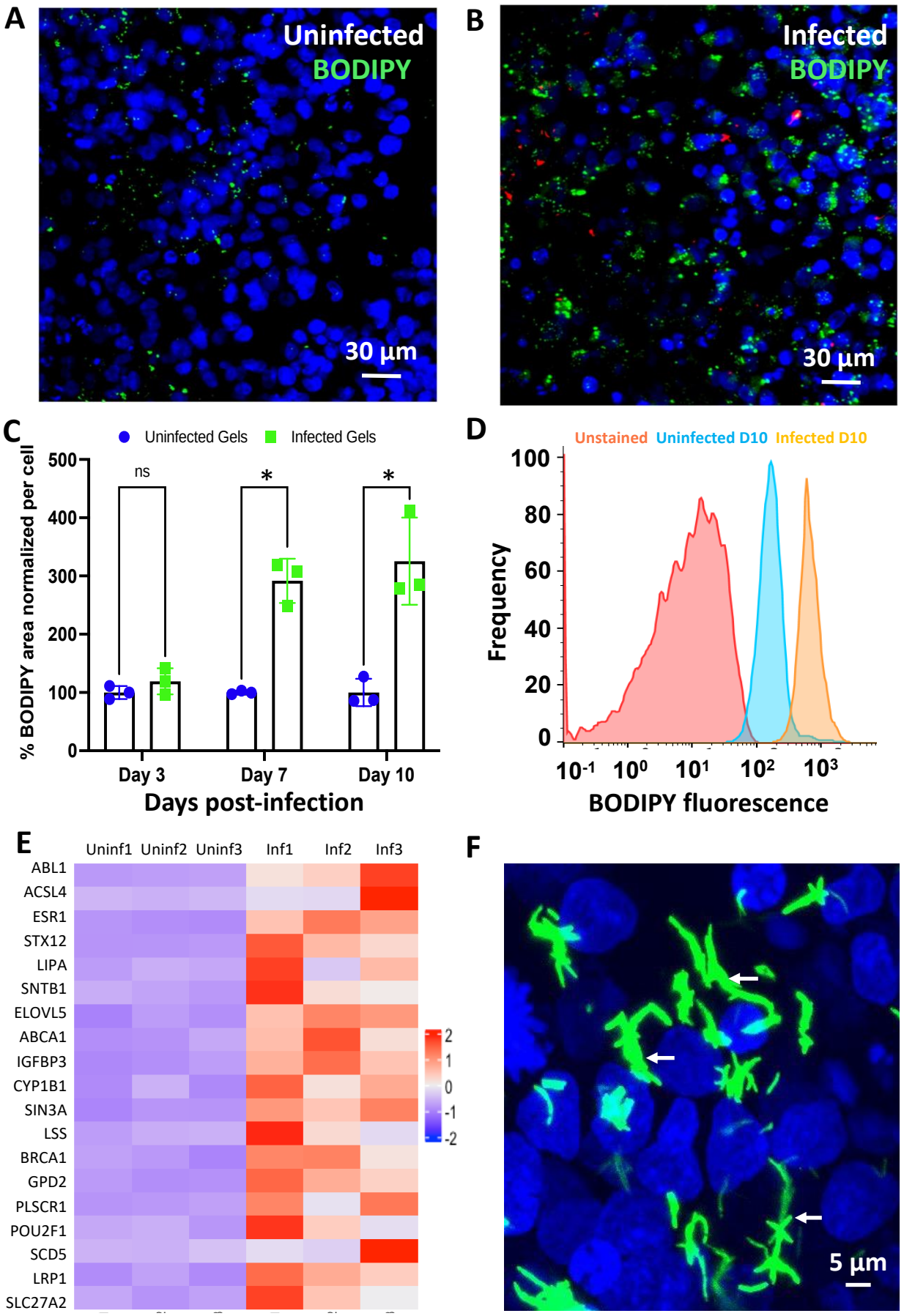
A
Uninfected
BODIPY
30 µm
B
Infected
BODIPY
30 µm
C
Uninfected Gels
Infected Gels
% BODIPY area normalized per cell
500
400
300
200
100
0
ns
*
*
Day 3
Day 7
Day 10
Days post-infection
D
Unstained
Uninfected D10
Infected D10
Frequency
100
80
60
40
20
0
10-1
100
101
102
103
BODIPY fluorescence
E
Uninf1
Uninf2
Uninf3
Inf1
Inf2
Inf3
ABL1
ACSL4
ESR1
STX12
LIPA
SNTB1
ELOVL5
ABCA1
IGFBP3
CYP1B1
SIN3A
LSS
BRCA1
GPD2
PLSCR1
POU2F1
SCD5
LRP1
SLC27A2
2
1
0
-1
-2
F
5 µm

Fig. 5 Cells in the infected collagen gels show accumulation of lipid bodies and differentiate to macrophages: Fluorescence microscopy images of uninfected gels (**A**) and gels infected with tdTomato expressing Mtb (red) (**B**) that were stained with the nuclear stain DAPI (blue) and BODIPY (green), 7 days post-infection. (**C**) Quantification of BODIPY staining using ImageJ showed infected gels with a higher stain area per mammalian cell (n = 3). (**D**) Flow cytometry histogram showing BODIPY expression: Unstained control (red), cells from uninfected gels day 10 (blue), cells from infected gels day 10 (orange). (**E**) Heat map of the average z-scores, showing the list of genes involved in lipid metabolism (common with a human caseous granuloma). (**F**) Fluorescence images showing that Mtb (green) forms complex cord-like structures in the infected collagen gels (highlighted using white arrows). For **C**, data in graphs represent the mean ± s.d., and p values were determined by two-tailed unpaired t-tests with Welch's correction for each time point using GraphPad Prism software. *p-value < 0.05 was considered significant. Day 7 (*p=0.012) and Day 10 (*p=0.026)

5. A more reliable drug screening platform – Elucidated by the efficacy of pyrazinamide:

Pyrazinamide (PZA) has been a mainstay of antituberculosis treatments since the 1950s and played a major role in shortening the therapy from 12 months to 6 months (*55, 56*). However, remarkably, it shows no significant activity in any *in vitro* model at clinically relevant concentrations (*57, 58*), and its anti-tubercular activity was discovered directly on an animal model of infection (*59, 60*), highlighting how the current *in vitro* culture systems are not optimal for drug testing. Given the exclusive effectivity of pyrazinamide *in vivo*, it has been difficult to fully understand its mechanism of action, and it is only in the recent past that some insights have emerged (*14, 61-65*).

Our study found that PZA consistently reduced the bacterial burden in our culture system at 50 µg/mL (**Fig. 6A**), which is in the range of average peak plasma concentration (C_{max}) in individuals undergoing TB treatment with PZA (*66*). We further validated this finding using primary human monocytes isolated from human PBMCs (**Fig. 6B**). However, at this concentration, PZA failed to act in 2D infection models (**Supplementary Fig. S7A**) and was also ineffective on planktonic bacteria and bacteria embedded in gels without mammalian cells (**Supplementary Fig. S7B-C**). The similar efficacy of pyrazinamide between our 3D collagen model and in *in vivo* conditions indicated the potential of our system as a more reliable drug testing platform.

Pyrazinamide is a prodrug catalyzed to its active form pyrazinoic acid (POA) by the bacterial gene *pncA* (*67*). One of the working hypotheses of PZA points to its ability to perturb the intrabacterial pH (*68*). Briefly, PZA gets metabolized to POA inside the bacteria and is transported out through the efflux pumps. However, in an acidic pH microenvironment (such as in a phagosome), POA gets protonated to HPOA, which then re-enters the bacteria. This cycle eventually leads to the bacteria being unable to maintain its cytoplasmic pH and membrane potential, leading to death. We tested this hypothesis by checking for phagosomal maturation in the infected 2D and 3D conditions and did not find any significant differences in colocalization of LAMP-1-stained lysosomes with Mtb in the 2D infection scenario compared to 3D, indicating a lesser probability for pH-dependent effectivity of PZA in the model **(Supplementary Fig. S8**).

Another interesting observation has been that PZA resistance in clinical samples is not always associated with mutations in *pncA* (*69-71*). A few studies have pointed to the critical role of Aspartate Decarboxylase *panD* and the Unfoldase *clpC1* genes in mediating resistance to PZA (*63, 64*). PanD is involved in the synthesis of pantothenic acid (vitamin B5), critical for

biosynthesis of coenzyme A and acyl carrier protein (ACP), involved in various steps of lipid metabolism, and hence bacterial mutants with deletion of these genes were found to be highly attenuated (*72*). The active form of the drug, POA, binds to PanD and the C-terminal end of the PanD-POA complex is recognized by the caseinolytic protease, ClpC1-ClpP, leading to its degradation (*61*). We tested for the same phenomenon in our system using four spontaneous POA mutants of H37Rv (*63*) and corroborated the previous findings that mutations were present in the *panD* gene corresponding to the C-terminal domain of PanD (**Supplementary Table 6**). *pncA* and *clpC1* genes did not have any mutations in these bacteria. We infected THP-1 cells with these POA mutants in the collagen gels and treated the experimental groups with PZA (50 µg/mL) (**Figs. 6C-F**). PZA was ineffective in reducing the bacterial burden for all 4 mutants, clearly emphasizing the critical role of PanD in the efficacy of PZA in the 3D model and strengthening the case for adopting this culture system in drug discovery and mechanistic studies.

Several other proteins are hypothesized to synergize/antagonize PZA activity (*73, 74*). We found that these Mtb genes were not differentially regulated in our gels compared to planktonic cultures (**Supplementary Table 8**). Thus, the transcriptomic data suggest that these proteins may have a minor role in PZA efficacy in our culture system, although there may be differences at the translational level. Further validation of the system was done using the other first-line anti-TB drugs (rifampicin, ethambutol, or isoniazid), which were also effective in reducing bacterial counts when used at their respective minimum inhibitory concentrations (MIC) of broth culture (**Supplementary Fig. S9 A-C**).

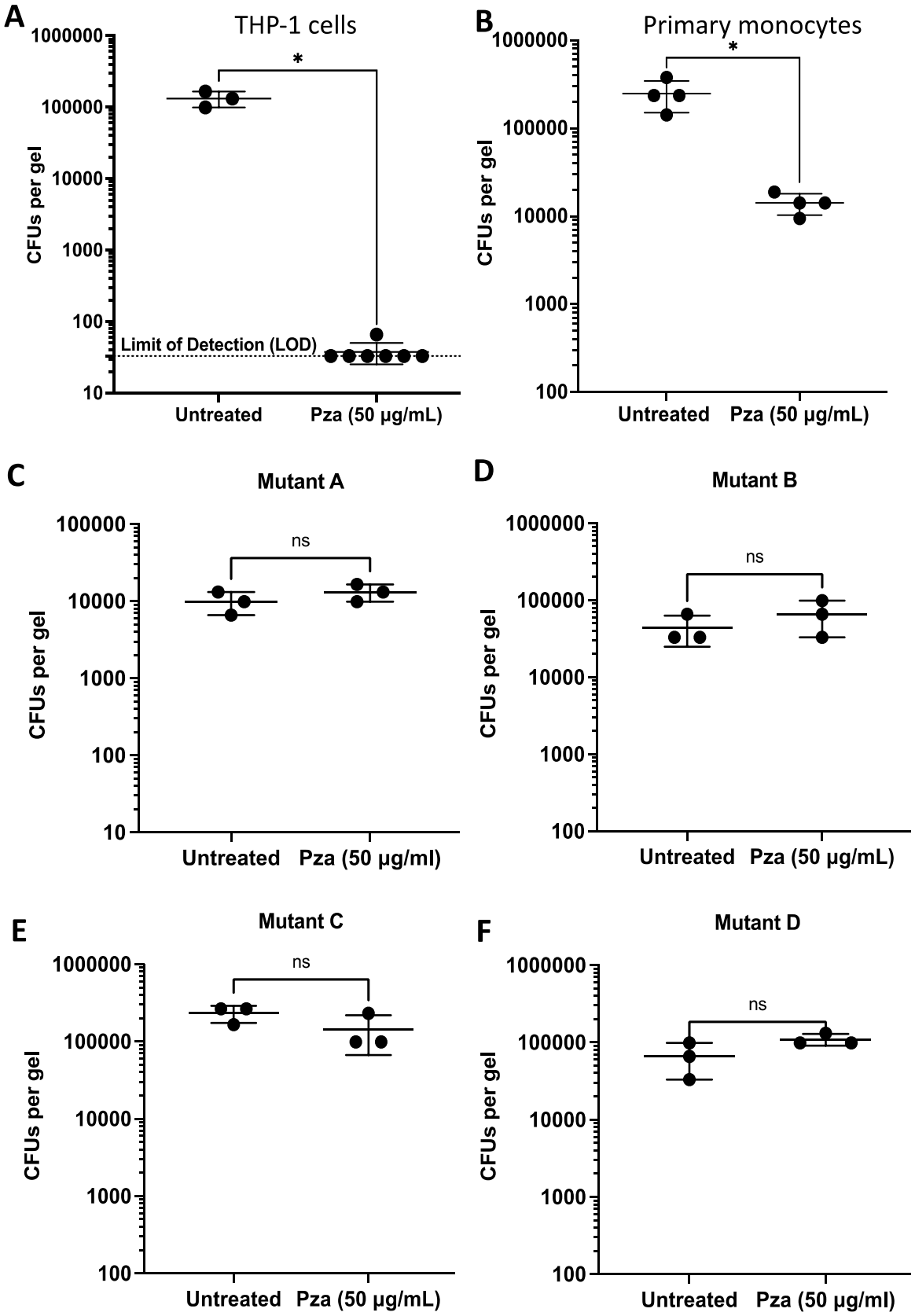
A
THP-1 cells
CFUs per gel
1000000
100000
10000
1000
100
10
*
Limit of Detection (LOD)
Untreated
Pza (50 µg/mL)
B
Primary monocytes
CFUs per gel
1000000
100000
10000
1000
100
*
Untreated
Pza (50 µg/mL)
C
Mutant A
CFUs per gel
100000
10000
1000
100
10
ns
Untreated
Pza (50 µg/ml)
D
Mutant B
CFUs per gel
1000000
100000
10000
1000
100
ns
Untreated
Pza (50 µg/mL)
E
Mutant C
CFUs per gel
1000000
100000
10000
1000
100
ns
Untreated
Pza (50 µg/mL)
F
Mutant D
CFUs per gel
1000000
100000
10000
1000
100
ns
Untreated
Pza (50 µg/ml)

Fig. 6 Pyrazinamide showed efficacy at clinically relevant concentration in infected collagen gels: CFU plots obtained after treating (**A**) Mtb infected THP-1 in collagen gels (n = 3 for uninfected and n = 7 for infected), (**B**) Mtb infected primary human monocytes (n = 4) and (**C, D, E & F**) Mtb (POA resistant strains) infected THP-1 cells with PZA at 50 µg/mL (ns: non-significant) (n = 3). Data in graphs represent the mean ± s.d., and p values were determined by two-tailed unpaired t-tests with Welch's correction using GraphPad Prism Software. p-value < 0.05 was considered significant. *p=0.0202 for **A** and *p=0.0171 for **B**. ns = non-significant for **C**-**F**.

Discussion:

Tuberculosis causes a significant social and economic burden on both patients and society. There is a need for active research to understand the bacteria-host interaction and find new drug candidates. Although experiments on planktonic cultures of Mtb and 2D infection experiments with mammalian cells continue to be the primary step for many studies, their inherent limitations often lead to findings that do not translate well to animal models and humans. Such efforts consume precious time and resources or could also curtail the development of effective therapies, warranting the need to develop better drug-testing platforms. In this study, we propose a 3D collagen-hydrogel culture system as a next-generation *in vitro* platform to delineate the complexities of Mtb infection by mimicking an *in vivo* system. 3D culture platforms are being extensively used to study many diseases and are gaining wide acceptance (*19*). The current culture system uses hydrogels made of collagen 1, the main ECM component of human lungs. ECM plays a fundamental role in TB pathogenesis during human infection, as Mtb is known to induce the production of matrix metalloproteases (MMPs), which digest collagen, leading to ECM degradation and disease progression (*75*). Hence, inhibitors that act on these proteases are being studied as potential supplements to the existing treatment

regimens (*76*). The 2D infection studies lack ECM, and mice are not known to produce orthologs of some MMPs found in humans (*77*). Among the various 3D platforms, a few studies have cultured peripheral blood mononuclear cells (PBMCs) with Mtb in a three-dimensional (3D) matrix to form micro aggregate structures of cells of nearly 100 µm surrounding an infected cell or bacteria (*16*) , and showed that collagen reduced mammalian cell death upon Mtb infection (*18*). Primary granulomas from zebrafish can be cultured *ex vivo* (*78*). More advanced 3D systems include engineering lung organoids using stem cells, though its potential is currently unexplored in TB research (*10*). Furthermore, *in vitro* hollow fibre system for TB (HFS-TB) was used to recapitulate the human pharmacokinetics and pharmacodynamics of a few TB drugs, which resulted in optimal dosing regimens for moxifloxacin and linezolid (*79*). Although these platforms add significant value to the field, there are difficulties in procuring primary lung granulomas, human PBMCs, and specialized equipment in BSL-3 containment. Furthermore, none of these systems has been able to show the efficacy of pyrazinamide at clinically relevant concentrations.

Hence, given the presence of natural ECM component like collagen, a suitable mechanical environment, and 3D culture, we believe that the 3D system proposed here is amenable to widespread adoption and will significantly contribute to testing and validating new hypotheses for transitioning from *in vitro* to *in vivo*. Collagen gels are easy to synthesize, widely used for many applications (*80*), and easy to work with even in BSL-3 facilities. These collagen gels have been extensively characterized and are modular, for example, the matrix characteristics, such as pore size, stiffness, etc., depend on polymerization temperature and can be tuned in accordance with human lung ECM (*81*).

THP-1 monocytes and BMDMs are commonly used for studying host-pathogen interaction *in vitro*, but the length scale of these studies continues to be a major challenge. BMDM infection offers a slightly longer duration to study host-pathogen interaction, and a previous study had

characterized the transcriptional and physiological profile of Mtb in infection with BMDMs for 14 days showing the adaptation of the pathogen in the face of host stress (*35*). However, the kinetics of the BMDMs response in terms of viability varies greatly with MOI, with approximately 75% at day 6, with an MOI of 1, which falls to less than 25% with an MOI of 5 (*82*). Our culture system also offers the flexibility of looking at host-pathogen interaction at multiple levels such as time (1 day – 3 weeks) and scale: single cell to multiple cells behaviour for mammalian and Mtb; and is suitable for analysis through tools such as genetic mutations in bacteria and host, histology, fluorescence microscopy, CFU assays, live-cell imaging, and flow cytometry.

We also show a genotypic and phenotypic similarity of mammalian cells in the infected collagen gels to human infection. For example, Mtb is known to induce the formation of lipid bodies in macrophages *in vivo* (*21, 83*). Previously, it has been shown that 2D infection of human macrophages can lead to a high accumulation of lipid bodies compared to uninfected macrophages (*84*), however, more recent reports indicate necrosis of other cells in the milieu to be critical for this phenomenon. An MOI of 1 or 5 in 2D cultures did not result in foamy macrophage formation but instead was seen with a high MOI of 50, which led to more than 60 % mammalian cell death (*85*). The necrotic factors served as a source of triglycerides for the live infected cells. Other commonly used methods include supplementation of oleate in the growth media to generate foamy macrophages, followed by infecting these cells with Mtb to study lipid retention/turnover (*86, 87*). Mtb infection of murine adipocytes (*88*) or supplementation with lipoproteins (*89*) have also been tried to induce the formation of foamy macrophages. This could explain the absence of foamy macrophages in our 2D infection as we used a low MOI of 1, which is unlikely to induce significant necrosis. In our collagen culture system, even a low burden of Mtb infection led to this phenotype without any additional supplementation of fatty acids. We also show cord-like Mtb replication in the infected collagen

gels, another prominent phenotype found *in vivo* (*22, 23, 49, 50*). Transcriptomic analysis of the mammalian cells in the infected collagen gels revealed a significantly greater overlap with human TB granulomas than in current culture systems. Such shortcomings in how mammalian cells in 2D respond to Mtb infection render them to be a somewhat unreliable systems for testing potential drug candidates. For example, none of the current *in vitro* systems could demonstrate any significant PZA efficacy at clinically relevant concentrations (≤ 50 µg/mL), which could be observed using our 3D collagen culture system. PZA has been shown efficacious *in vitro* using planktonic bacteria at a pH of 5.95, with the MIC of 200 µg/mL (*68*). Further reduction in pH of medium resulted in growth inhibition of several strains of bacteria (*68*). Similarly, in human monocyte-derived macrophages, treatment with concentrations as high as 100-400 µg/mL of PZA only resulted in about 70% reduction in bacteria as determined by fluorescence imaging (*65, 90*). Thus, our platform is potentially an excellent substitute for current *in vitro* models and a starting point for more accurate drug testing and to give deeper insights into host-pathogen interaction before large-scale animal studies are performed.

The tuberculosis bacilli in a host are taken up by monocytes, macrophages, dendritic cells, and neutrophils (*7*) and also have a niche in mesenchymal stem cells (*91*). A limitation of our model is that most of the data generated is on the THP-1 cell line. In our culture, PZA was also efficacious when used on Mtb infected primary human monocytes, however other observations regarding mammalian and bacterial phenotypes needs to be validated with primary cells. Another limitation is that these cultures do not incorporate other immune and non-immune cells known to be relevant *in vivo*. During infection, Mtb primarily resides in alveolar macrophages (AM) and interstitial macrophages (IM) *in vivo* and has distinct interactions with each of these macrophage populations (*9*); AMs offer a more permissive niche for bacterial growth compared to IMs (*44*), and hence, it would be interesting to see how AMs respond to infection in our collagen hydrogels. However, there are no established human AM cell lines,

and primary AMs are very difficult to obtain., Furthermore, the bacteria encounter multiple stresses *in vivo*, such as adaptive immune response and hypoxia in a necrotic granulomatous core, which was not present in our platform. The absence of other components of the adaptive immune system also means that Mtb can continue to proliferate in the macrophages as the duration of infection progresses. It is possible to increase the density of cells cultured in collagen gels, which may lead to low oxygen concentration near the center of the gel, as shown in spheroid cultures (*92*) and will be explored in future studies.

Conclusions:

We show that our 3D collagen cell culture model offers a significantly longer window for studying host-pathogen interaction. Cells in the infected microenvironment have properties similar to cells in *in vivo*, in terms of lipid accumulation, cord formation, and gene expression, among other characteristics. The effectivity of pyrazinamide, a first in any *in vitro* model, in reducing the bacterial burden further emphasizes the robustness of the platform, and we hypothesize that potentially undiscovered mechanistic phenomena can be unravelled using our culture system. The system offers utility with ease of usage and modularity while incorporating resources that are easily accessible to the research community and can therefore be readily adopted.

Methods:

1. **Culture of mammalian cells and isolation of primary human monocytes**

Human THP-1 monocytes were seeded at a concentration of 10^5 cells/mL and passaged every 3 days. The cells were cultured in RPMI 1640 media containing 10% Fetal bovine serum (FBS) and antibiotics (Penicillin/Streptomycin) and grown in a humidified incubator supplemented with CO_2 and maintained at 37 $^{\circ}$C.

For human primary monocytes, 10 mL of whole blood was collected from volunteers (Institutional Human Ethics Committee Approval Number: 20-14012020) and peripheral blood mononuclear cells (PBMCs) were isolated by density gradient centrifugation over Histopaque®-1077 (Sigma Aldrich). From these PBMCs, the primary monocytes were isolated using a monocyte isolation kit (Mojosort™ Human CD14+ Monocytes Isolation Kit, BioLegend®), per the manufacturer's instructions. These primary monocytes were cultured in RPMI 1640 media supplemented with 10% FBS.

2. Culture of H37Rv

Mycobacterium tuberculosis strain H37Rv was cultured in media composed of 7H9, tween 80 (0.05%), glycerol (0.1%) with albumin-dextrose-catalase (ADC) (10%) enrichment at 37 °C. GFP-H37Rv carrying the plasmid pmyc1tetO-gfp, tetR(B), and tdTomato H37Rv carrying the plasmid pTEC27 (pMSP12: tdTomato), with hygromycin (50 μg/mL) as the selection marker, were used for imaging and flow cytometry experiments.

3. Collagen gel preparation

Rat tail Collagen I (3 mg/mL, Gibco™) was used. Collagen gels with final concentrations of 1 mg/mL to 2 mg/mL were made as per manufacturer's recommendations. The pH of these gels ranged from 7-7.4. The polymerization was carried out in a humidified incubator at 37 °C for 20 minutes, following which they were transferred into a 24-well plate containing 1X phosphate buffered saline (PBS). In experiments involving mammalian cells and bacteria, the cell suspension was added in place of 1X PBS, and the gels were transferred to wells containing RPMI 1640 containing 10% FBS.

4. Infection experiments

Infected collagen gels were made as follows: single-cell suspension of H37Rv (OD of 0.5-1) was prepared and added to THP-1 cells at a multiplicity of infection (MOI) of 40:1 (bacteria : mammalian cells) in the required volume for making the gels. Post gelation, the infection was

carried out for 12 h, after which amikacin sulfate (200 µg/mL) was added to the media for 6 h to remove extracellular bacteria. The media was changed every 48 h during the experiment. The gels were treated with collagenase, type 1 (0.4 mg/mL, GIBCO™) for 1 h at 37 °C to degrade the collagen for flow cytometry experiments. The cells were stained with LIVE/DEAD™ (L34955 LIVE/DEAD™ Fixable Violet Dead Cell Stain Kit, for 405 nm excitation), followed by fixation with 4% paraformaldehyde (PFA), and used for further analysis.

For 2D infection experiments, THP-1 cells were differentiated into adherent macrophages using 20 nM Phorbol 12-Myristate 13-Acetate (PMA). Briefly, cells were incubated in media containing PMA for 24 h, post which the PMA was removed and the cells were allowed to rest for 2 days with fresh media. Cells were then infected with Mtb at an MOI of 1:1 (bacteria: mammalian cells) for 4 h and treated with amikacin sulfate for 2 h.

5. Mtb growth kinetics

To study the kinetics of Mtb replication during infection in the hydrogel system, we infected THP-1 cells with H37Rv carrying the replication clock plasmid, pBP10 (*36*) (a kind gift from Dr. David Sherman). Intracellular CFUs were carried out by treating the gels with collagenase, lysing the mammalian cells with 0.1% Triton X-100, followed by spotting serial dilutions on Middlebrook 7H11 agar plates supplemented with 10% OADC, with and without 30 µg/mL kanamycin and incubated at 37 ºC for 20-24 days. The replication and death rates of Mtb were quantified using the mathematical model proposed by Gill et al.(*36*)

6. Second-harmonic imaging of collagen gels and lung tissues from mice

Second-harmonic generation (SHG) images of the samples were acquired using a mode-locked fiber laser (Coherent Fidelity HP) with an operational wavelength of 1040 nm, a pulse width of 140 fs, and a repetition rate of 80 MHz. The incident beam was scanned using a galvo-scanner (GVS001, Thorlabs), with the beam focused on the sample using a 60x/1.2 NA water

immersion objective (UPLSAPO60XW, Olympus). A photomultiplier tube (R3896, Hamamatsu) was used to collect the SHG emission from collagen. The incident power at the focus for imaging collagen was 1.7 mW. The average pore size of the collagen gels was calculated using the particle analyzer in the BoneJ plugin of ImageJ (NIH, USA). The resolution of the microscope was around 400 nm, and hence the pores below the size of 0.16 μm^2 were excluded from the analysis.

7. Atomic Force Microscopy (AFM) measurement

Collagen gels were loaded into a custom polydimethylsiloxane (PDMS)-based AFM holder. The sample was kept hydrated during measurement, and indentation (with a depth of 500 microns) was done at different points using Park Systems NX-10 AFM in a liquid medium. Force distance spectroscopy was carried out using the HYDRA6V-200NG-TL cantilever with a 5 µm diameter sphere. The force constant was 0.045 N/m, and the force limit was 0.91 nN. The up and down speed was 0.3 µm/s. The data generated were further analyzed through a custom-written MATLAB code to determine Young's modulus (*28*).

8. TB antibiotic treatments:

THP-1 cells were infected with Mtb in collagen gels for 7 days, post which the gels in the treatment group were treated with the first line of antituberculosis drugs – rifampicin (0.3 µg/mL), isoniazid (0.25 µg/mL), and ethambutol (5 µg/mL). At 3- and 7-days post-treatment, gels were degraded with collagenase, and cells were lysed with 0.1% Triton X-100. Cell lysates were plated on 7H11 plates supplemented with 10% OADC and incubated at 37° C. The CFUs were counted 3-4 weeks after plating. For studying pyrazinamide (50 µg/mL) efficacy, the infection was carried out for either 4 or 7 days, post which the cells were treated for 6 or 3 days, respectively.

9. Generation of pyrazinoic acid (POA) mutants:

The H37Rv POA mutants were generated as described by Pooja et.al. (*61*). Briefly, Mtb was grown on 7H11 plates supplemented with 2 mM POA and 10% OADC, and a few colonies were picked and restreaked on fresh 2 mM POA plates. Colonies from 2nd plate were further grown in 7H9 media supplemented with 2 mM POA and 10% ADC. Genomic DNA was isolated from these mutants and sequenced with gene-specific primer pairs (**Supplementary Table 7**) for *pncA, panD, clpC1* genes using Phusion^{TM} High-Fidelity DNA polymerase (Thermo Scientific^{TM}) as per the manufacturer's instructions. The products were sequenced using Sanger sequencing and the results were analyzed using the NCBI BLAST tool.

10. Antibody & BODIPY staining:

Differentiation of monocytes to macrophages was quantified by CD68 expression. Briefly, cells in the infected and uninfected hydrogels released using collagenase (0.4 mg/mL). The cells were stained with LIVE/DEAD^{TM} (L34955 LIVE/DEAD™ Fixable Violet Dead Cell Stain Kit, for 405 nm excitation), post which they fixed using 4% PFA. The cells were then permeabilized using 0.1% Triton X-100 and stained with anti-CD68 antibody (PE-Mouse Anti-Human CD68 set, BD Biosciences) (1:50 dilution) overnight in a buffer made of 1X PBS supplemented with 1% bovine serum albumin (BSA).

To study the localization of Mtb phagosomes with lysosomes in the infected 2D and 3D scenarios, cells were stained with anti-(LAMP-1) antibody (ab24170, Abcam). Briefly, the cells in 2D were incubated in a blocking buffer made of 1X PBS supplemented with 1 % BSA, 0.1% Triton X-100 and 5% donkey serum for two hours at room temperature. The cells were then washed with PBS and stained with the primary antibody (0.5 μg/mL) diluted in the blocking buffer and incubated at 4 °C overnight. This was followed by staining with the secondary antibody (Donkey anti-Rabbit IgG (H+L) Highly Cross-Adsorbed Secondary Antibody, Alexa Fluor™ Plus 647) diluted in the blocking buffer (1 μg/mL), for 3 hours and imaged at 60X using a fluorescence microscope (IN Cell Analyzer 6000). For LAMP-1 staining

in hydrogels, the gels were fixed with 4% PFA, post which cryo-sectioning (*93*) was carried out. The sections were stained with primary and secondary antibodies similar to 2D cultures. For the 2D infection, analysis was done on day 3 and 5 post-infection, while for 3D, it was done on day 5 and 7 post-infection.

For staining the mammalian cells in 2D and in the hydrogels with BODIPY™ 493/503 (Thermo Scientific™), the cells were fixed with 4 % PFA for 1 hr followed by incubation with the dye diluted in 1X PBS (1 µg/mL) for 15 mins at 37 °C. The dye was washed, followed by staining with Hoechst 3342 (Thermo Scientific™) and imaged using a fluorescence microscope (IN Cell Analyzer 6000) with a 40X objective.

For all the flow cytometry experiments, the cells were suspended in 300 µL of FACS buffer and data was acquired using BD FACSDiva™ software, followed by analysis using FlowJo (v9). The gating strategy to identify the suitable cell populations for CD68 and BODIPY staining is shown in **Supplementary Fig. S10** and for the viability assay in **Supplementary Fig. S11.**

11. Preparation of samples for dual RNA-sequencing:

The gels were degraded using collagenase (0.4 mg/mL) at day 14. The cells were then treated with Guanidinium thiocyanate buffer (GTC buffer) containing beta-mercaptoethanol. The homogenate was centrifuged at 5000 g resulting in pellets of Mtb. The supernatant was collected and processed for THP-1 RNA extraction. Mtb RNA was isolated from the pellet using FastRNA® Pro Blue kit (MP Biomedicals™) as per the manufacturer's recommendations. Briefly, 1 mL of RNApro™ solution was added to the bacterial pellet and was transferred to a lysing matrix tube. Bead beating was carried using a FastPrep® instrument (2 cycles of 20 seconds each at a speed setting of 4.5 m/s). The isolated RNA was purified using a NucleoSpin RNA kit (MACHEREY-NAGEL) per the manufacturer's recommendations

and quantified using a NanoDrop™ One/One^{C} Microvolume UV-Vis Spectrophotometer (Thermo Scientific^{TM}).

12. Bioinformatic pipeline

The libraries were paired-end sequenced on Illumina HiSeq X Ten sequencer for 150 cycles (Illumina, San Diego, USA) following the manufacturer's instructions. The data obtained from the sequencing run was de-multiplexed using Bcl2fastq software v2.20, and FastQ files were generated based on the unique dual barcode sequences. The sequencing quality was assessed using FastQC v0.11.8 software. The adapter sequences were trimmed, bases above Q30 were considered, and low-quality bases were filtered off during read pre-processing and used for downstream analysis. The pre-processed high-quality data were aligned to the human reference genome using HISAT with the default parameters to identify the alignment percentage. Reads were classified into aligned (which align to the reference genome) and unaligned reads. The tool featureCount was used to estimate and calculate transcript abundance. Absolute counts for transcripts were identified and used in differential expression calculations. DESeq was used to calculate the differentially expressed transcripts. Transcripts were categorized into up, down, and neutrally regulated based on the log2fold change (log2fc) cutoff of ±1 value, and with a false-discovery rate (FDR) < 0.05 were selected for further analysis.

The following publicly available data sets were used for analysis: GSE162729 – for THP-1 macrophages; GSE20050 – for human caseous granuloma, GSE17443 – for lymph node granulomas and GSE174566 -2D PBMCs. From these data sets, genes with a |log2fc|>1 having a false-discovery rate (FDR)<0.05 were selected for further analysis. The ReactomePA package in R was used for gene ontology enrichment analysis of the differentially regulated genes (*94*). For the human caseous and lymph node granulomas, the significantly enriched ($p<0.05$) commonly regulated (upregulated and downregulated) REACTOME pathways in either one or

both the data sets were selected for representation. Heatmaps were made using the ComplexHeatmap function in R.

13. Statistical analysis:

Data were presented as mean ± standard deviation and plotted using GraphPad PRISM 9 software. Measurements for each data point were taken from distinct samples. Unpaired two-tailed t-tests with or without Welch's correction were used to detect statistical differences between groups depending on the number of variables, with $p < 0.05$ considered significant.

Acknowledgements:

We thank Dr. David Russell (Cornell University) for providing valuable external feedback on this manuscript. We thank Dr. Deepak Saini (IISc) for providing us with GFP and tdTomato conjugated stains of H37Rv and Dr. Amit Singh (IISc) and Dr. Narendra Dixit (IISc) for their invaluable inputs on this project. We thank the Centre for Infectious Diseases Research (CIDR) at IISc Bangalore for allowing us to carry out the studies in the Biosafety Level-3 facility. We thank Dr. Siddharth Jhunjhunwala (IISc) for access to the flow cytometer. We also acknowledge Dr. Thomas Dick's (Center for Discovery and Innovation, Hackensack Meridian Health) advice for generating spontaneous mutants of PanD. The fluorescence image acquisition was carried out at the Microbiology and Cell Biology (MCB) imaging facility at the Indian Institute of Science**.**

Funding:

This work was supported by the Wellcome Trust–DBT India Alliance Intermediate Fellowship to RA (IA/I/20/1/504906), Mr. Lakshmi Narayanan, and the Indian Institute of Science start-up fund. We also thank Dr. Vijaya and Rajagopal Rao for funding Biomedical Engineering research at the Centre for BioSystems Science and Engineering.

Data Availability: The datasets generated during and/or analyzed during the current study are available from the corresponding author on reasonable request. RNA sequencing data is being uploaded to GSE database and will be soon made publicly available.

Author contributions:

RA and VG wrote the manuscript. RA and VG designed experiments. APS helped with the initial optimization of collagen gels. VG performed experiments and analyzed the results. APS and JKM performed the second-harmonic generation and 2-photon imaging. SJ helped with characterizing the POA mutants.

Competing interests:

The authors declare no conflict of interest.

References:

1. E. Harding, WHO global progress report on tuberculosis elimination. *The Lancet. Respiratory medicine* **8**, 19 (2020); published online EpubJan (10.1016/S2213-2600(19)30418-7).
2. J. D. Ernst, The immunological life cycle of tuberculosis. *Nature reviews. Immunology* **12**, 581-591 (2012); published online EpubJul 13 (10.1038/nri3259).
3. S. B. Cohen, B. H. Gern, J. L. Delahaye, K. N. Adams, C. R. Plumlee, J. K. Winkler, D. R. Sherman, M. Y. Gerner, K. B. Urdahl, Alveolar Macrophages Provide an Early Mycobacterium tuberculosis Niche and Initiate Dissemination. *Cell Host Microbe* **24**, 439-446 e434 (2018); published online EpubSep 12 (10.1016/j.chom.2018.08.001).
4. M. Samstein, H. A. Schreiber, I. M. Leiner, B. Susac, M. S. Glickman, E. G. Pamer, Essential yet limited role for CCR2(+) inflammatory monocytes during Mycobacterium tuberculosis-specific T cell priming. *Elife* **2**, e01086 (2013); published online EpubNov 12 (10.7554/eLife.01086).
5. C. J. Cambier, S. M. O'Leary, M. P. O'Sullivan, J. Keane, L. Ramakrishnan, Phenolic Glycolipid Facilitates Mycobacterial Escape from Microbicidal Tissue-Resident Macrophages. *Immunity* **47**, 552-565 e554 (2017); published online EpubSep 19 (10.1016/j.immuni.2017.08.003).
6. A. I. Rovetta, D. Pena, R. E. Hernandez Del Pino, G. M. Recalde, J. Pellegrini, F. Bigi, R. M. Musella, D. J. Palmero, M. Gutierrez, M. I. Colombo, V. E. Garcia, IFNG-mediated immune responses enhance autophagy against Mycobacterium tuberculosis antigens in patients with active tuberculosis. *Autophagy* **10**, 2109-2121 (2014)10.4161/15548627.2014.981791).
7. C. Bussi, M. G. Gutierrez, Mycobacterium tuberculosis infection of host cells in space and time. *FEMS Microbiol Rev* **43**, 341-361 (2019); published online EpubJul 1 (10.1093/femsre/fuz006).
8. X. Bai, S. H. Kim, T. Azam, M. T. McGibney, H. Huang, C. A. Dinarello, E. D. Chan, IL-32 is a host protective cytokine against Mycobacterium tuberculosis in

differentiated THP-1 human macrophages. *J Immunol* **184**, 3830-3840 (2010); published online EpubApr 1 (10.4049/jimmunol.0901913).
9. D. Pisu, L. Huang, J. K. Grenier, D. G. Russell, Dual RNA-Seq of Mtb-Infected Macrophages In Vivo Reveals Ontologically Distinct Host-Pathogen Interactions. *Cell Rep* **30**, 335-350 e334 (2020); published online EpubJan 14 (10.1016/j.celrep.2019.12.033).
10. K. L. Fonseca, P. N. S. Rodrigues, I. A. S. Olsson, M. Saraiva, Experimental study of tuberculosis: From animal models to complex cell systems and organoids. *PLoS Pathog.* **13**, e1006421 (2017); published online EpubAug (10.1371/journal.ppat.1006421).
11. M. Kapalczynska, T. Kolenda, W. Przybyla, M. Zajaczkowska, A. Teresiak, V. Filas, M. Ibbs, R. Blizniak, L. Luczewski, K. Lamperska, 2D and 3D cell cultures - a comparison of different types of cancer cell cultures. *Archives of medical science : AMS* **14**, 910-919 (2018); published online EpubJun (10.5114/aoms.2016.63743).
12. D. Mahamed, M. Boulle, Y. Ganga, C. Mc Arthur, S. Skroch, L. Oom, O. Catinas, K. Pillay, M. Naicker, S. Rampersad, C. Mathonsi, J. Hunter, E. B. Wong, M. Suleman, G. Sreejit, A. S. Pym, G. Lustig, A. Sigal, Intracellular growth of Mycobacterium tuberculosis after macrophage cell death leads to serial killing of host cells. *Elife* **6**, (2017); published online EpubJan 28 (10.7554/eLife.22028).
13. M. T. Reichmann, L. B. Tezera, A. F. Vallejo, M. Vukmirovic, R. Xiao, J. Reynolds, S. Jogai, S. Wilson, B. Marshall, M. G. Jones, A. Leslie, J. M. D'Armiento, N. Kaminski, M. E. Polak, P. Elkington, Integrated transcriptomic analysis of human tuberculosis granulomas and a biomimetic model identifies therapeutic targets. *J. Clin. Invest.* **131**, (2021); published online EpubAug 2 (10.1172/JCI148136).
14. Q. Sun, X. Li, L. M. Perez, W. Shi, Y. Zhang, J. C. Sacchettini, The molecular basis of pyrazinamide activity on Mycobacterium tuberculosis PanD. *Nat Commun* **11**, 339 (2020); published online EpubJan 17 (10.1038/s41467-019-14238-3).
15. T. Gumbo, A. J. Lenaerts, D. Hanna, K. Romero, E. Nuermberger, Nonclinical models for antituberculosis drug development: a landscape analysis. *The Journal of infectious diseases* **211 Suppl 3**, S83-95 (2015); published online EpubJun 15 (10.1093/infdis/jiv183).
16. L. E. Fitzgerald, N. Abendano, R. A. Juste, M. Alonso-Hearn, Three-dimensional in vitro models of granuloma to study bacteria-host interactions, drug-susceptibility, and resuscitation of dormant mycobacteria. *BioMed research international* **2014**, 623856 (2014)10.1155/2014/623856).
17. N. Kapoor, S. Pawar, T. D. Sirakova, C. Deb, W. L. Warren, P. E. Kolattukudy, Human granuloma in vitro model, for TB dormancy and resuscitation. *PLoS One* **8**, e53657 (2013)10.1371/journal.pone.0053657).
18. L. B. Tezera, M. K. Bielecka, A. Chancellor, M. T. Reichmann, B. A. Shammari, P. Brace, A. Batty, A. Tocheva, S. Jogai, B. G. Marshall, M. Tebruegge, S. N. Jayasinghe, S. Mansour, P. T. Elkington, Dissection of the host-pathogen interaction in human tuberculosis using a bioengineered 3-dimensional model. *Elife* **6**, (2017); published online EpubJan 07 (10.7554/eLife.21283).
19. M. A. Schwartz, C. S. Chen, Cell biology. Deconstructing dimensionality. *Science* **339**, 402-404 (2013); published online EpubJan 25 (10.1126/science.1233814).
20. F. Pampaloni, E. G. Reynaud, E. H. Stelzer, The third dimension bridges the gap between cell culture and live tissue. *Nat Rev Mol Cell Biol* **8**, 839-845 (2007); published online EpubOct (10.1038/nrm2236).
21. M. J. Kim, H. C. Wainwright, M. Locketz, L. G. Bekker, G. B. Walther, C. Dittrich, A. Visser, W. Wang, F. F. Hsu, U. Wiehart, L. Tsenova, G. Kaplan, D. G. Russell,

Caseation of human tuberculosis granulomas correlates with elevated host lipid metabolism. *EMBO Mol. Med.* **2**, 258-274 (2010); published online EpubJul (10.1002/emmm.201000079).
22. A. J. Pagan, C. T. Yang, J. Cameron, L. E. Swaim, F. Ellett, G. J. Lieschke, L. Ramakrishnan, Myeloid Growth Factors Promote Resistance to Mycobacterial Infection by Curtailing Granuloma Necrosis through Macrophage Replenishment. *Cell Host Microbe* **18**, 15-26 (2015); published online EpubJul 8 (10.1016/j.chom.2015.06.008).
23. R. D. Berg, S. Levitte, M. P. O'Sullivan, S. M. O'Leary, C. J. Cambier, J. Cameron, K. K. Takaki, C. B. Moens, D. M. Tobin, J. Keane, L. Ramakrishnan, Lysosomal Disorders Drive Susceptibility to Tuberculosis by Compromising Macrophage Migration. *Cell* **165**, 139-152 (2016); published online EpubMar 24 (10.1016/j.cell.2016.02.034).
24. A. J. Pagan, L. J. Lee, J. Edwards-Hicks, C. B. Moens, D. M. Tobin, E. M. Busch-Nentwich, E. L. Pearce, L. Ramakrishnan, mTOR-regulated mitochondrial metabolism limits mycobacterium-induced cytotoxicity. *Cell* **185**, 3720-3738 e3713 (2022); published online EpubSep 29 (10.1016/j.cell.2022.08.018).
25. C. B. Raub, V. Suresh, T. Krasieva, J. Lyubovitsky, J. D. Mih, A. J. Putnam, B. J. Tromberg, S. C. George, Noninvasive assessment of collagen gel microstructure and mechanics using multiphoton microscopy. *Biophys J* **92**, 2212-2222 (2007); published online EpubMar 15 (10.1529/biophysj.106.097998).
26. P. Hameed, G. Manivasagam, An overview of bio-actuation in collagen hydrogels: a mechanobiological phenomenon. *Biophys Rev* **13**, 387-403 (2021); published online EpubJun (10.1007/s12551-021-00804-x).
27. D. Sicard, A. J. Haak, K. M. Choi, A. R. Craig, L. E. Fredenburgh, D. J. Tschumperlin, Aging and anatomical variations in lung tissue stiffness. *Am J Physiol Lung Cell Mol Physiol* **314**, L946-L955 (2018); published online EpubJun 1 (10.1152/ajplung.00415.2017).
28. S. R. Polio, A. N. Kundu, C. E. Dougan, N. P. Birch, D. E. Aurian-Blajeni, J. D. Schiffman, A. J. Crosby, S. R. Peyton, Cross-platform mechanical characterization of lung tissue. *PLoS One* **13**, e0204765 (2018)10.1371/journal.pone.0204765).
29. X. Chen, O. Nadiarynkh, S. Plotnikov, P. J. Campagnola, Second harmonic generation microscopy for quantitative analysis of collagen fibrillar structure. *Nature protocols* **7**, 654-669 (2012); published online EpubMar 8 (10.1038/nprot.2012.009).
30. T. Abraham, J. A. Hirota, S. Wadsworth, D. A. Knight, Minimally invasive multiphoton and harmonic generation imaging of extracellular matrix structures in lung airway and related diseases. *Pulm Pharmacol Ther* **24**, 487-496 (2011); published online EpubOct (10.1016/j.pupt.2011.03.008).
31. C. L. Buchheit, R. R. Rayavarapu, Z. T. Schafer, The regulation of cancer cell death and metabolism by extracellular matrix attachment. *Semin Cell Dev Biol* **23**, 402-411 (2012); published online EpubJun (10.1016/j.semcdb.2012.04.007).
32. B. Al Shammari, T. Shiomi, L. Tezera, M. K. Bielecka, V. Workman, T. Sathyamoorthy, F. Mauri, S. N. Jayasinghe, B. D. Robertson, J. D'Armiento, J. S. Friedland, P. T. Elkington, The Extracellular Matrix Regulates Granuloma Necrosis in Tuberculosis. *J. Infect. Dis.* **212**, 463-473 (2015); published online EpubAug 1 (10.1093/infdis/jiv076).
33. H. Haas, J. Michel, T. G. Sacks, In vitro susceptibility of mycobacteria species other than Mycobacterium tuberculosis to amikacin, cephalosporins and cefoxitin. *Chemotherapy* **28**, 1-5 (1982)10.1159/000238053).

34. T. Parish, In vitro drug discovery models for Mycobacterium tuberculosis relevant for host infection. *Expert Opin Drug Discov* **15**, 349-358 (2020); published online EpubMar (10.1080/17460441.2020.1707801).
35. K. H. Rohde, D. F. Veiga, S. Caldwell, G. Balazsi, D. G. Russell, Linking the transcriptional profiles and the physiological states of Mycobacterium tuberculosis during an extended intracellular infection. *PLoS Pathog.* **8**, e1002769 (2012)10.1371/journal.ppat.1002769).
36. W. P. Gill, N. S. Harik, M. R. Whiddon, R. P. Liao, J. E. Mittler, D. R. Sherman, A replication clock for Mycobacterium tuberculosis. *Nat Med* **15**, 211-214 (2009); published online EpubFeb (10.1038/nm.1915).
37. S. Srivastava, J. D. Ernst, L. Desvignes, Beyond macrophages: the diversity of mononuclear cells in tuberculosis. *Immunol Rev* **262**, 179-192 (2014); published online EpubNov (10.1111/imr.12217).
38. F. Geissmann, M. G. Manz, S. Jung, M. H. Sieweke, M. Merad, K. Ley, Development of monocytes, macrophages, and dendritic cells. *Science* **327**, 656-661 (2010); published online EpubFeb 5 (10.1126/science.1178331).
39. D. A. Chistiakov, M. C. Killingsworth, V. A. Myasoedova, A. N. Orekhov, Y. V. Bobryshev, CD68/macrosialin: not just a histochemical marker. *Laboratory investigation; a journal of technical methods and pathology* **97**, 4-13 (2017); published online EpubJan (10.1038/labinvest.2016.116).
40. P. Fontan, V. Aris, S. Ghanny, P. Soteropoulos, I. Smith, Global transcriptional profile of Mycobacterium tuberculosis during THP-1 human macrophage infection. *Infect. Immun.* **76**, 717-725 (2008); published online EpubFeb (10.1128/IAI.00974-07).
41. N. Shimono, L. Morici, N. Casali, S. Cantrell, B. Sidders, S. Ehrt, L. W. Riley, Hypervirulent mutant of Mycobacterium tuberculosis resulting from disruption of the mce1 operon. *Proc Natl Acad Sci U S A* **100**, 15918-15923 (2003); published online EpubDec 23 (10.1073/pnas.2433882100).
42. E. V. Nazarova, C. R. Montague, T. La, K. M. Wilburn, N. Sukumar, W. Lee, S. Caldwell, D. G. Russell, B. C. VanderVen, Rv3723/LucA coordinates fatty acid and cholesterol uptake in Mycobacterium tuberculosis. *Elife* **6**, (2017); published online EpubJun 27 (10.7554/eLife.26969).
43. E. V. Nazarova, C. R. Montague, L. Huang, T. La, D. Russell, B. C. VanderVen, The genetic requirements of fatty acid import by Mycobacterium tuberculosis within macrophages. *Elife* **8**, (2019); published online EpubFeb 8 (10.7554/eLife.43621).
44. L. Huang, E. V. Nazarova, S. Tan, Y. Liu, D. G. Russell, Growth of Mycobacterium tuberculosis in vivo segregates with host macrophage metabolism and ontogeny. *J Exp Med* **215**, 1135-1152 (2018); published online EpubApr 2 (10.1084/jem.20172020).
45. Y. J. Zhang, M. C. Reddy, T. R. Ioerger, A. C. Rothchild, V. Dartois, B. M. Schuster, A. Trauner, D. Wallis, S. Galaviz, C. Huttenhower, J. C. Sacchettini, S. M. Behar, E. J. Rubin, Tryptophan biosynthesis protects mycobacteria from CD4 T-cell-mediated killing. *Cell* **155**, 1296-1308 (2013); published online EpubDec 5 (10.1016/j.cell.2013.10.045).
46. D. F. Warner, Mycobacterium tuberculosis metabolism. *Cold Spring Harb Perspect Med* **5**, (2014); published online EpubDec 11 (10.1101/cshperspect.a021121).
47. S. Ehrt, D. Schnappinger, K. Y. Rhee, Metabolic principles of persistence and pathogenicity in Mycobacterium tuberculosis. *Nature reviews. Microbiology* **16**, 496-507 (2018); published online EpubAug (10.1038/s41579-018-0013-4).

48. G. Li, J. Li, Y. Otsuka, S. Zhang, M. Takahashi, K. Yamada, A BODIPY-Based Fluorogenic Probe for Specific Imaging of Lipid Droplets. *Materials* **13**, (2020); published online EpubFeb 3 (10.3390/ma13030677).
49. E. G. Ufimtseva, N. I. Eremeeva, E. M. Petrunina, T. V. Umpeleva, S. I. Bayborodin, D. V. Vakhrusheva, S. N. Skornyakov, Mycobacterium tuberculosis cording in alveolar macrophages of patients with pulmonary tuberculosis is likely associated with increased mycobacterial virulence. *Tuberculosis (Edinb)* **112**, 1-10 (2018); published online EpubSep (10.1016/j.tube.2018.07.001).
50. H. Clay, H. E. Volkman, L. Ramakrishnan, Tumor necrosis factor signaling mediates resistance to mycobacteria by inhibiting bacterial growth and macrophage death. *Immunity* **29**, 283-294 (2008); published online EpubAug 15 (10.1016/j.immuni.2008.06.011).
51. F. J. Roca, L. J. Whitworth, H. A. Prag, M. P. Murphy, L. Ramakrishnan, Tumor necrosis factor induces pathogenic mitochondrial ROS in tuberculosis through reverse electron transport. *Science* **376**, eabh2841 (2022); published online EpubJun 24 (10.1126/science.abh2841).
52. A. Bernut, J. L. Herrmann, K. Kissa, J. F. Dubremetz, J. L. Gaillard, G. Lutfalla, L. Kremer, Mycobacterium abscessus cording prevents phagocytosis and promotes abscess formation. *Proc Natl Acad Sci U S A* **111**, E943-952 (2014); published online EpubMar 11 (10.1073/pnas.1321390111).
53. T. R. Lerner, C. J. Queval, R. P. Lai, M. R. Russell, A. Fearns, D. J. Greenwood, L. Collinson, R. J. Wilkinson, M. G. Gutierrez, Mycobacterium tuberculosis cords within lymphatic endothelial cells to evade host immunity. *JCI Insight* **5**, (2020); published online EpubMay 21 (10.1172/jci.insight.136937).
54. J. T. Belisle, V. D. Vissa, T. Sievert, K. Takayama, P. J. Brennan, G. S. Besra, Role of the major antigen of Mycobacterium tuberculosis in cell wall biogenesis. *Science* **276**, 1420-1422 (1997); published online EpubMay 30 (10.1126/science.276.5317.1420).
55. Controlled clinical trial of four short-course (6-month) regimens of chemotherapy for treatment of pulmonary tuberculosis. Third report. East African-British Medical Research Councils. *Lancet* **2**, 237-240 (1974); published online EpubAug 3 (
56. Controlled trial of 6-month and 8-month regimens in the treatment of pulmonary tuberculosis. First report. *Am Rev Respir Dis* **118**, 219-228 (1978); published online EpubAug (10.1164/arrd.1978.118.2.219).
57. M. S. Tarshis, W. A. Weed, Jr., Lack of significant in vitro sensitivity of Mycobacterium tuberculosis to pyrazinamide on three different solid media. *Am Rev Tuberc* **67**, 391-395 (1953); published online EpubMar (10.1164/art.1953.67.3.391).
58. Y. Zhang, W. Shi, W. Zhang, D. Mitchison, Mechanisms of Pyrazinamide Action and Resistance. *Microbiol Spectr* **2**, MGM2-0023-2013 (2014); published online EpubAug (10.1128/microbiolspec.MGM2-0023-2013).
59. R. M. McCune, Jr., W. McDermott, R. Tompsett, The fate of Mycobacterium tuberculosis in mouse tissues as determined by the microbial enumeration technique. II. The conversion of tuberculous infection to the latent state by the administration of pyrazinamide and a companion drug. *J Exp Med* **104**, 763-802 (1956); published online EpubNov 1 (10.1084/jem.104.5.763).
60. L. Malone, A. Schurr, H. Lindh, K. D. Mc, J. S. Kiser, J. H. Williams, The effect of pyrazinamide (aldinamide) on experimental tuberculosis in mice. *Am Rev Tuberc* **65**, 511-518 (1952); published online EpubMay (
61. P. Gopal, R. Tasneen, M. Yee, J. P. Lanoix, J. Sarathy, G. Rasic, L. Li, V. Dartois, E. Nuermberger, T. Dick, In Vivo-Selected Pyrazinoic Acid-Resistant Mycobacterium

tuberculosis Strains Harbor Missense Mutations in the Aspartate Decarboxylase PanD and the Unfoldase ClpC1. *ACS Infect Dis* **3**, 492-501 (2017); published online EpubJul 14 (10.1021/acsinfecdis.7b00017).
62. M. Yee, P. Gopal, T. Dick, Missense Mutations in the Unfoldase ClpC1 of the Caseinolytic Protease Complex Are Associated with Pyrazinamide Resistance in Mycobacterium tuberculosis. *Antimicrob Agents Chemother* **61**, (2017); published online EpubFeb (10.1128/AAC.02342-16).
63. P. Gopal, W. Nartey, P. Ragunathan, J. Sarathy, F. Kaya, M. Yee, C. Setzer, M. S. S. Manimekalai, V. Dartois, G. Gruber, T. Dick, Pyrazinoic Acid Inhibits Mycobacterial Coenzyme A Biosynthesis by Binding to Aspartate Decarboxylase PanD. *ACS Infect Dis* **3**, 807-819 (2017); published online EpubNov 10 (10.1021/acsinfecdis.7b00079).
64. P. Gopal, J. P. Sarathy, M. Yee, P. Ragunathan, J. Shin, S. Bhushan, J. Zhu, T. Akopian, O. Kandror, T. K. Lim, M. Gengenbacher, Q. Lin, E. J. Rubin, G. Gruber, T. Dick, Pyrazinamide triggers degradation of its target aspartate decarboxylase. *Nat Commun* **11**, 1661 (2020); published online EpubApr 3 (10.1038/s41467-020-15516-1).
65. P. Santucci, D. J. Greenwood, A. Fearns, K. Chen, H. Jiang, M. G. Gutierrez, Intracellular localisation of Mycobacterium tuberculosis affects efficacy of the antibiotic pyrazinamide. *Nat Commun* **12**, 3816 (2021); published online EpubJun 21 (10.1038/s41467-021-24127-3).
66. E. Nuermberger, J. Grosset, Pharmacokinetic and pharmacodynamic issues in the treatment of mycobacterial infections. *European journal of clinical microbiology & infectious diseases : official publication of the European Society of Clinical Microbiology* **23**, 243-255 (2004); published online EpubApr (10.1007/s10096-004-1109-5).
67. P. Jureen, J. Werngren, J. C. Toro, S. Hoffner, Pyrazinamide resistance and pncA gene mutations in Mycobacterium tuberculosis. *Antimicrob Agents Chemother* **52**, 1852-1854 (2008); published online EpubMay (10.1128/AAC.00110-08).
68. M. Salfinger, L. B. Heifets, Determination of pyrazinamide MICs for Mycobacterium tuberculosis at different pHs by the radiometric method. *Antimicrob Agents Chemother* **32**, 1002-1004 (1988); published online EpubJul (10.1128/AAC.32.7.1002).
69. N. Casali, V. Nikolayevskyy, Y. Balabanova, S. R. Harris, O. Ignatyeva, I. Kontsevaya, J. Corander, J. Bryant, J. Parkhill, S. Nejentsev, R. D. Horstmann, T. Brown, F. Drobniewski, Evolution and transmission of drug-resistant tuberculosis in a Russian population. *Nat Genet* **46**, 279-286 (2014); published online EpubMar (10.1038/ng.2878).
70. K. Stoffels, V. Mathys, M. Fauville-Dufaux, R. Wintjens, P. Bifani, Systematic analysis of pyrazinamide-resistant spontaneous mutants and clinical isolates of Mycobacterium tuberculosis. *Antimicrob Agents Chemother* **56**, 5186-5193 (2012); published online EpubOct (10.1128/AAC.05385-11).
71. S. Zhang, J. Chen, W. Shi, W. Liu, W. Zhang, Y. Zhang, Mutations in panD encoding aspartate decarboxylase are associated with pyrazinamide resistance in Mycobacterium tuberculosis. *Emerg Microbes Infect* **2**, e34 (2013); published online EpubJun (10.1038/emi.2013.38).
72. V. K. Sambandamurthy, X. Wang, B. Chen, R. G. Russell, S. Derrick, F. M. Collins, S. L. Morris, W. R. Jacobs, Jr., A pantothenate auxotroph of Mycobacterium tuberculosis is highly attenuated and protects mice against tuberculosis. *Nat Med* **8**, 1171-1174 (2002); published online EpubOct (10.1038/nm765).

73. P. Gopal, G. Gruber, V. Dartois, T. Dick, Pharmacological and Molecular Mechanisms Behind the Sterilizing Activity of Pyrazinamide. *Trends Pharmacol Sci* **40**, 930-940 (2019); published online EpubDec (10.1016/j.tips.2019.10.005).
74. J. M. Thiede, N. A. Dillon, M. D. Howe, R. Aflakpui, S. J. Modlin, S. E. Hoffner, F. Valafar, Y. Minato, A. D. Baughn, Pyrazinamide Susceptibility Is Driven by Activation of the SigE-Dependent Cell Envelope Stress Response in Mycobacterium tuberculosis. *mBio* **13**, e00439-00421 (2022)doi:10.1128/mbio.00439-21).
75. P. T. Elkington, J. M. D'Armiento, J. S. Friedland, Tuberculosis immunopathology: the neglected role of extracellular matrix destruction. *Sci. Transl. Med.* **3**, 71ps76 (2011); published online EpubFeb 23 (10.1126/scitranslmed.3001847).
76. Y. Xu, L. Wang, M. D. Zimmerman, K. Y. Chen, L. Huang, D. J. Fu, F. Kaya, N. Rakhilin, E. V. Nazarova, P. Bu, V. Dartois, D. G. Russell, X. Shen, Matrix metalloproteinase inhibitors enhance the efficacy of frontline drugs against Mycobacterium tuberculosis. *PLoS Pathog.* **14**, e1006974 (2018); published online EpubApr (10.1371/journal.ppat.1006974).
77. B. C. Jackson, D. W. Nebert, V. Vasiliou, Update of human and mouse matrix metalloproteinase families. *Hum Genomics* **4**, 194-201 (2010); published online EpubFeb (10.1186/1479-7364-4-3-194).
78. M. R. Cronan, M. A. Matty, A. F. Rosenberg, L. Blanc, C. J. Pyle, S. T. Espenschied, J. F. Rawls, V. Dartois, D. M. Tobin, An explant technique for high-resolution imaging and manipulation of mycobacterial granulomas. *Nat. Methods* **15**, 1098-1107 (2018); published online EpubDec (10.1038/s41592-018-0215-8).
79. J. G. Pasipanodya, E. Nuermberger, K. Romero, D. Hanna, T. Gumbo, Systematic Analysis of Hollow Fiber Model of Tuberculosis Experiments. *Clin Infect Dis* **61 Suppl 1**, S10-17 (2015); published online EpubAug 15 (10.1093/cid/civ425).
80. S. R. Caliari, J. A. Burdick, A practical guide to hydrogels for cell culture. *Nat Methods* **13**, 405-414 (2016); published online EpubApr 28 (10.1038/nmeth.3839).
81. A. D. Doyle, Generation of 3D Collagen Gels with Controlled Diverse Architectures. *Current protocols in cell biology* **72**, 10 20 11-10 20 16 (2016); published online EpubSep 1 (10.1002/cpcb.9).
82. L. Zhang, X. Jiang, D. Pfau, Y. Ling, C. F. Nathan, Type I interferon signaling mediates Mycobacterium tuberculosis-induced macrophage death. *J Exp Med* **218**, (2021); published online EpubFeb 1 (10.1084/jem.20200887).
83. D. G. Russell, P. J. Cardona, M. J. Kim, S. Allain, F. Altare, Foamy macrophages and the progression of the human tuberculosis granuloma. *Nat Immunol* **10**, 943-948 (2009); published online EpubSep (10.1038/ni.1781).
84. V. Singh, S. Jamwal, R. Jain, P. Verma, R. Gokhale, K. V. Rao, Mycobacterium tuberculosis-driven targeted recalibration of macrophage lipid homeostasis promotes the foamy phenotype. *Cell Host Microbe* **12**, 669-681 (2012); published online EpubNov 15 (10.1016/j.chom.2012.09.012).
85. N. Jaisinghani, S. Dawa, K. Singh, A. Nandy, D. Menon, P. D. Bhandari, G. Khare, A. Tyagi, S. Gandotra, Necrosis Driven Triglyceride Synthesis Primes Macrophages for Inflammation During Mycobacterium tuberculosis Infection. *Front Immunol* **9**, 1490 (2018)10.3389/fimmu.2018.01490).
86. W. Lee, B. C. VanderVen, R. J. Fahey, D. G. Russell, Intracellular Mycobacterium tuberculosis exploits host-derived fatty acids to limit metabolic stress. *J Biol Chem* **288**, 6788-6800 (2013); published online EpubMar 8 (10.1074/jbc.M112.445056).
87. M. Podinovskaia, W. Lee, S. Caldwell, D. G. Russell, Infection of macrophages with Mycobacterium tuberculosis induces global modifications to phagosomal function. *Cell Microbiol* **15**, 843-859 (2013); published online EpubJun (10.1111/cmi.12092).

88. P. Agarwal, S. R. Khan, S. C. Verma, M. Beg, K. Singh, K. Mitra, A. N. Gaikwad, M. S. Akhtar, M. Y. Krishnan, Mycobacterium tuberculosis persistence in various adipose depots of infected mice and the effect of anti-tubercular therapy. *Microbes Infect* **16**, 571-580 (2014); published online EpubJul (10.1016/j.micinf.2014.04.006).
89. I. Caire-Brandli, A. Papadopoulos, W. Malaga, D. Marais, S. Canaan, L. Thilo, C. de Chastellier, Reversible lipid accumulation and associated division arrest of Mycobacterium avium in lipoprotein-induced foamy macrophages may resemble key events during latency and reactivation of tuberculosis. *Infect Immun* **82**, 476-490 (2014); published online EpubFeb (10.1128/IAI.01196-13).
90. P. Santucci, B. Aylan, L. Botella, E. M. Bernard, C. Bussi, E. Pellegrino, N. Athanasiadi, M. G. Gutierrez, Visualizing Pyrazinamide Action by Live Single-Cell Imaging of Phagosome Acidification and Mycobacterium tuberculosis pH Homeostasis. *mBio* **13**, e0011722 (2022); published online EpubApr 26 (10.1128/mbio.00117-22).
91. N. Jain, H. Kalam, L. Singh, V. Sharma, S. Kedia, P. Das, V. Ahuja, D. Kumar, Mesenchymal stem cells offer a drug-tolerant and immune-privileged niche to Mycobacterium tuberculosis. *Nat Commun* **11**, 3062 (2020); published online EpubJun 16 (10.1038/s41467-020-16877-3).
92. D. J. Richards, Y. Li, C. M. Kerr, J. Yao, G. C. Beeson, R. C. Coyle, X. Chen, J. Jia, B. Damon, R. Wilson, E. Starr Hazard, G. Hardiman, D. R. Menick, C. C. Beeson, H. Yao, T. Ye, Y. Mei, Human cardiac organoids for the modelling of myocardial infarction and drug cardiotoxicity. *Nat Biomed Eng* **4**, 446-462 (2020); published online EpubApr (10.1038/s41551-020-0539-4).
93. C. C. Yang, L. Jenkins, K. J. L. Burg, Adapted Cryosectioning Method for Hydrogels Used in Regenerative Medicine. *Journal of Histotechnology* **30**, 185-191 (2007); published online Epub2007/09/01 (10.1179/his.2007.30.3.185).
94. G. Yu, Q. Y. He, ReactomePA: an R/Bioconductor package for reactome pathway analysis and visualization. *Mol Biosyst* **12**, 477-479 (2016); published online EpubFeb (10.1039/c5mb00663e).